Walport, F., Kucukler, M., and Gardner, L. (2022). Stability design of stainless steel structures. *Journal of Structural Engineering ASCE*, 148(1); 04021225.

https://doi.org/10.1061/(ASCE)ST.1943-541X.0003165

# Stability design of stainless steel structures

- F. Walport<sup>1</sup>, M. Kucukler<sup>2</sup> and L. Gardner<sup>3</sup>
- <sup>1</sup>Research Associate, Dept. of Civil and Environmental Engineering, Imperial College London, London,
- 4 U.K. (corresponding author). E-mail: fiona.walport12@imperial.ac.uk
- <sup>2</sup>Assistant Professor, School of Engineering, University of Warwick, Coventry, U.K. E-mail:
- 6 merih.kucukler@warwick.ac.uk
- <sup>3</sup>Professor of Structural Engineering, Dept. of Civil and Environmental Engineering, Imperial College
- 8 London, London, U.K. E-mail: leroy.gardner@imperial.ac.uk

## 9 **ABSTRACT**

10

11

12

13

14

15

16

17

18

19

20

21

22

23

24

25

26

27

28

29

1

The direct analysis method (DAM), featuring second order elastic analysis with two stiffness reduction factors -  $\tau_b$  and  $\tau_g$ , is the primary means of stability design for steel structures in AISC 360 and AISI S100. The equivalent provisions for stainless steel structures, which are due to be incorporated into the upcoming AISC 370 and ASCE-8 Specifications are developed herein. Stainless steel exhibits a rounded stress-strain response, typically described by the Ramberg-Osgood formulation. The slope of this function (i.e. the tangent modulus), adjusted to consider the influence of residual stresses, is used to define the stiffness reduction factor  $\tau_b$  at a given axial load level to be applied to members in compression to allow for the adverse influence of the spread of plasticity and residual stresses. The dependency of the degree of stiffness reduction on the roundedness of the stress-strain curve, which varies between the different grades of stainless steel is also directly captured through the strain hardening exponent n that features in the Ramberg–Osgood formulation. Values of 0.7 for AISC 370 and 0.9 for ASCE-8 are proposed for the general stiffness reduction factor  $\tau_g$  to be applied to all member stiffnesses to account for the development and spread of plasticity, and to ensure a suitable reduction in stiffness for slender members with low axial load levels. The different  $\tau_g$  values between the two specifications is required to reflect the different buckling curves and axial-bending interaction expressions employed. The accuracy of the proposed method for the design of stainless steel members and frames is assessed through comparisons with benchmark shell finite element results. Comparisons are also made against the new provisions in AISC 370 for design by second order inelastic analysis. The reliability of the design proposals is demonstrated through statistical analyses, where it is shown that a resistance factor  $\phi$  of 0.9 can be adopted.

Keywords: AISC 370; Inelastic buckling; Stability; Stainless steel; Stiffness reduction; Structural

31 design.

30

32

33

34

35

36

37

38

39

40

41

42

43

44

45

46

47

48

49

50

51

52

53

54

55

56

57

58

59

## INTRODUCTION

The direct analysis method (DAM) in AISC 360 (AISC, 2016b) and AISI S100 (AISI, 2016) uses second order analysis to determine the internal forces in structures in the deformed configuration. The influence of material nonlinearity and residual stresses can be accounted for by either (1) performing an elastic analysis but with reduced stiffness in the members or (2) performing an inelastic analysis. In the former case, the relative simplicity of elastic analysis is retained, while in the latter case, more accurate results are achieved. The capacity of members is verified by either (1) buckling checks or (2), if initial bow imperfections are included in the members of the analysed structure, cross-section checks. In either case, the need for the determination of effective buckling lengths is eliminated (Deierlein, 2003; Kucukler, Gardner & Macorini, 2014; Surovek-Maleck & White, 2004a; Chan, Liu & Liu, 2011). Frame out-of-plumbness is accounted for in the analysis through direct modelling or through the application of notional loads. For design by second order elastic analysis, also referred to as geometrically nonlinear analysis (GNA), two stiffness reduction factors are defined: (1) a general stiffness reduction factor with a value of 0.8, referred to herein as  $\tau_g$ , to be applied to all member stiffnesses to account for the development and spread of plasticity and (2)  $\tau_b$ , to account for the additional reduction in flexural stiffness due to the effects of yielding and residual stresses of heavily loaded compression members. The value of  $\tau_g = 0.8$  also ensures that the strength of slender members is similar to that obtained from column buckling curves (Deierlein, 2003). Further studies have been carried out to derive a single stiffness reduction factor  $\tau_{MN}$  that considers fully the detrimental influence of spread of plasticity, residual stresses and member out-of-straightness on structural behavior for both steel (Kucukler, Gardner & Macorini, 2014, 2016, 2015; Kucukler & Gardner, 2018, 2019) and stainless steel (Shen & Chacón, 2020b, 2020a). Design by elastic analysis with stiffness reduction has been developed and widely used for carbon steel structures (Surovek-Maleck & White, 2004a, 2004b; Deierlein, 2003). However, no equivalent design rules are available for application to stainless steel structures, where the influence of material yielding is more significant (Walport et al., 2019). The new AISC 370 Specification (AISC, 2021) will encompass the design, fabrication and erection of hot-rolled and welded austenitic and duplex stainless steel structures. The provisions closely mirror AISC 360 (AISC, 2016b), but deviate where necessary

60 to account for the differences in material behavior between stainless steel and carbon steel and the

resulting influence on structural behavior (Baddoo & Francis, 2014; SCI, 2013). Meanwhile, ASCE-8

62 (ASCE, 2021), for the design of cold-formed austenitic, duplex and ferritic stainless steel structures,

which is broadly aligned to AISI S100 (AISI, 2016), is also being substantially revised.

In this paper, stiffness reduction factors are derived to enable extension of the direct analysis method to

the stability design of stainless steel structures. The accuracy of the proposed stiffness reduction method

in predicting the capacity of austenitic, duplex and ferritic stainless steel members and frames is

assessed relative to benchmark shell finite element results obtained second order inelastic analysis with

imperfections – also referred to as geometrically and materially nonlinear analysis with imperfections

(GMNIA). Comparisons are also made against a new method of design by second order inelastic

analysis (GMNIA) with strain limits, which is due to be incorporated into AISC 370 (AISC, 2021;

Walport, Gardner & Nethercot, 2021). The reliability of the design proposals is demonstrated through

statistical analyses, and worked examples are presented to illustrate their application.

## FINITE ELEMENT MODELLING

61

63

65

66

67

68

69

70

71

72

73

75

76

77

78

79

80

82

84

85

86

87

88

74 Both shell and beam finite element (FE) models are developed in this study; the shell FE models are

utilized to generate benchmark results with which to assess the accuracy of the proposed design

approach, while the beam FE models are used in the application of the stiffness reduction method. In

this section, details of the FE modelling approach employed are presented. The FE models were

developed using the general purpose FE software ABAQUS (ABAQUS, 2014) and validated against

experimental results from the literature, as reported below.

#### **Development of Benchmark Shell Finite Element Models**

81 The generation of benchmark shell finite element results, obtained by means of second order inelastic

analysis with imperfections (GMNIA), is described in this section. The four-noded reduced integration

83 S4R shell element, from the ABAQUS (ABAQUS, 2014) element library, was employed herein to

create all benchmark models, as successfully adopted in previous similar studies (Meng & Gardner,

2020; Kucukler, Gardner & Macorini, 2015; Bu & Gardner, 2019a). Both welded I-sections and cold-

formed hollow sections were modeled, with the web depth and flange width subdivided into 12 elements

to accurately capture local buckling and the spread of plasticity. The web plate was offset by half the

thickness of each of the flanges such that overlapping of the flange and web plates was avoided. The

number of elements along the length of the members was defined such that the element aspect ratio was close to unity. The modified Riks method was used to trace the full load-deformation response of the modeled members and frames. Pin and roller support conditions were achieved through the coupling of the member end cross-section nodes to a master node, and in all cases the members were constrained out-of-plane along the flange centrelines at intervals close to the local buckling half-wavelength  $L_{el}$  (Fieber, Gardner & Macorini, 2019b). Note that, mirroring the approach taken in the development of the equivalent provisions in AISI S100, only cold-formed hollow sections are modeled herein. It is recommended that open cross-sections are considered in future research.

Geometric imperfections and residual stresses

In the benchmark models, an initial out-of-straightness in the form of a half-sine wave with a magnitude  $e_0$  of 1/1000 of the member length L was assumed. For the frames, an initial out-of-plumbness of 1/500 of the frame height was assumed, as recommended in (AISC, 2016a), and applied as a notional load ( $H_{NL}$ ). The geometric imperfections were incorporated into the models in the most unfavourable directions considering the applied loading and boundary conditions. Sinusoidal local plate imperfections were defined with an imperfection magnitude of 1/200 and 1/50 of the web height and half flange width, respectively, as recommended in EN 1993-1-5 (EN 1993-1-5, 2009), and a half-wavelength close to the elastic local buckling half-wavelength  $L_{\rm b,cs}$ , calculated using the formulae set out in Fieber, Gardner & Macorini (2019b).

For the I-section models, the residual stress distribution for welded stainless steel I-sections developed by Yuan et al. (2014) was utilized, noting that stainless steel I-sections are predominately produced by welding. The residual stresses were modeled explicitly as an initial stress condition; corresponding plastic strains were also assigned (Kucukler, Xing & Gardner, 2020). An additional analysis step was included prior to loading to allow the residual stresses to equilibrate. Based on previous experimental and numerical findings (Ellobody & Young, 2005; Gardner & Nethercot, 2004; Jandera, Gardner & Machacek, 2008), residual stresses were not included in the hollow section FE models.

## Material modeling

The stress-strain behavior of the modeled members and frames was described using the two-stage Ramberg-Osgood formulation (Arrayago, Real & Gardner, 2015; Mirambell & Real, 2000), as given by Eqs. (1) and (2):

118 
$$\varepsilon = \frac{f}{E} + 0.002 \left(\frac{f}{F_{v}}\right)^{n} \quad \text{for} \quad f \le F_{y}$$
 (1)

119 
$$\varepsilon = 0.002 + \frac{F_y}{E} + \frac{f - F_y}{E_{Ty}} + \left(\varepsilon_u - 0.002 - \frac{F_y}{E} - \frac{F_u - F_y}{E_{Ty}}\right) \left(\frac{f - F_y}{F_u - F_y}\right)^m \quad \text{for} \quad F_y < f \le F_u$$
 (2)

where  $\varepsilon$  and f are the engineering strain and stress respectively,  $F_y$  is the yield (0.2% proof) stress, E is the Young's modulus,  $F_u$  is the ultimate stress,  $E_{Ty}$  is the tangent modulus at the yield (0.2% proof) stress, defined by Eq. (3),  $\varepsilon_u$  is the ultimate strain estimated as  $\varepsilon_u = 1 - F_y/F_u$  for austenitic and duplex stainless steel and as  $\varepsilon_u = 0.6(1 - F_y/F_u)$  for ferritic stainless steel, and n and m are the strain hardening exponents. In this study, typical grades of austenitic, duplex and ferritic stainless steel have been considered and the key material properties recommended in (AISC, 2021; ASCE, 2021) have been adopted, as summarised in Table 1.

$$E_{Ty} = \frac{E}{1 + 0.002 n_{\overline{F_y}}^E} \tag{3}$$

128 Validation of shell finite element models

120

121

122

123

124

125

126

129

130

131

132

133

134

135

136

137

138

139

140

141

142

143

144

145

To validate the adopted shell finite element modeling approach, the 12 experiments of (Bu & Gardner, 2019b) on austenitic stainless steel I-section beam-columns were simulated. The testing comprised pinended members under uniaxial major or minor axis bending plus compression, with the initial loading eccentricities varied to provide a range of moment-to-axial load ratios. For the minor axis bending cases, the member slenderness  $L/r_v$ , where L is the member length and  $r_v$  is the radius of gyration about the minor axis, was equal to 95.9; for the major axis bending cases, the member slenderness  $L/r_x$ , where  $r_x$ is the radius of gyration about the major axis, was equal 57.0. The measured geometry and local and global imperfection amplitudes were incorporated into the FE models, along with the measured stressstrain response. Fig. 1 shows the experimental and numerical lateral deflection paths for five (three buckling about the major axis and two about the minor axis) of the 12 cases; the responses are consistently in close agreement. In terms of the failure load predictions, the mean FE-to-test ultimate load ratio was 0.99 and 0.98 for the six major and six minor cases, respectively, with corresponding COV values of 0.057 and 0.053, respectively. In addition to the accurate capacity predictions demonstrated herein, the adopted shell FE modeling approach has also been shown to provide accurate results in a number of previous studies (Meng & Gardner, 2020; Kucukler, Gardner & Macorini, 2015; Bu & Gardner, 2019a). The shell FE models are thus considered to be suitable for the generation of benchmark results against which to assess the design provisions proposed in this paper.

## **Development of Beam Finite Element Models**

146

147

148

149

150

151

152

153

154

155

156

157

158

159

160

165

The 2-noded linear Timoshenko beam elements B31OS and B31, from the ABAQUS element library, were employed to create beam FE models with open and closed cross-sections, respectively, for implementation of the proposed design approach. Models were created of columns, beams, beam-columns and frames. In the developed frame models, the members were connected via fixed multi-point constraint ties at their ends providing full continuity. Results from the beam FE models were compared against those from shell FE models to ensure that the key member-level and frame-level behavioral features were accurately captured; this is demonstrated in Fig. 2, where load-deformation paths of an example austenitic stainless steel fixed based portal frame are compared. To account for the finite size of the rigid beam-to-column connections in the benchmark shell FE simulations, the member lengths in the beam FE models were shortened and rigid \*MPC, Beam links were used to represent the connection region, as shown in Fig. 2a (Fieber, Gardner & Macorini, 2020). It can be seen that the shell and beam FE models provide essentially the same global response predictions.

#### DERIVATION OF STIFFNESS REDUCTION FACTORS FOR DESIGN BY SECOND ORDER

## ELASTIC ANALYSIS

- 161 In this section, stiffness reduction factors for the design of stainless steel structures by second order
- elastic analysis (GNA) are derived. The factors are derived in line with those for carbon steel members
- set out in AISC 360 (AISC, 2016b), but reflect the particular characteristics of stainless steel. The
- proposals are due to be incorporated into AISC 370 (AISC, 2021) and ASCE-8 (ASCE, 2021).

## Stiffness Reduction Factor $\tau_b$

- The stiffness reduction factor  $\tau_b$  accounts for the effects of yielding and residual stresses on the flexural
- stiffness of compression members; it should be applied by reducing the moment of inertia (second
- moment of area) of the columns and is a function of the level of axial loading.
- 169 Existing provisions for steel structures
- In AISC 360 (AISC, 2016b), the stiffness reduction factor  $\tau_b$  is given by Eq. (4) for steel structures and
- was derived from the Column Research Council (CRC) column strength curve (Lui & Ge, 2005), where
- 172  $P_r$  is the required axial compressive strength using LRFD or ASD load combinations and  $P_{ns}$  is the
- cross-section compressive strength; for nonslender sections  $P_{ns} = F_y A_g$ , where  $F_y$  is the yield stress and

*A* is cross-sectional area, and for slender sections  $P_{ns} = F_y A_e$ , where  $A_e$  is the effective cross-sectional area.

176 
$$\tau_b = \begin{cases} 1.0 & \frac{P_r}{P_{ns}} \le 0.5\\ 4\left(\frac{P_r}{P_{ns}}\right)\left(1 - \frac{P_r}{P_{ns}}\right) & \frac{P_r}{P_{ns}} > 0.5 \end{cases}$$
(4)

The expression was obtained from the ratio of the inelastic to the elastic column buckling capacity (Yura, 1971; Liew, 1992), which can, broadly, be considered to follow the tangent modulus concept (Liew, White & Chen, 1994; Orbison, 1982; Liew, 1992; Deierlein, 2003; Lui & Ge, 2005). The reduction factor reflects the material behavior of carbon steel and the presence of residual stresses; for axial load levels less than half of the cross-section yield load, there is no stiffness reduction. Stiffness reduction commences beyond this value as plasticity develops at the outer fibres of the cross-section owing to the presence of residual stresses with peak values in compression assumed to be equal to one-half of the yield strength  $F_y$  (Orbison, 1982). The level of stiffness reduction increases under increasing axial load. Since  $\tau_b$  is a function of the axial load level, it must be applied iteratively in the design process; the resulting forces and moments from the analysis are only true at the load level assumed in the calculation of  $\tau_b$ . However, this step is often not needed because for steel design,  $\tau_b$  only applies at relatively high axial load levels  $P/P_{ns} > 0.5$  (Surovek-Maleck & White, 2004a). Since Eq. (4) i.e. the CRC column curve does not consider member out-of-straightness in its derivation, allowance for these bow imperfections is needed either through member checks or through direct modelling in the analysis.

Development of new provisions for stainless steel structures

A stiffness reduction function for stainless steel compression members to account for the influence of plasticity  $\tau_{b,m}$  can be directly derived from the Ramberg-Osgood expression (Eq. (1)). Defining the stiffness reduction factor due to material nonlinearity as the ratio of the tangent to the Young's modulus,  $\tau_{b,m} = E_t/E$ , where  $E_t = df/d\varepsilon$  and f = P/A, the following expression is obtained:

196 
$$\tau_{b,m} = \frac{1}{1 + 0.002 n_{F_y}^E \left(\frac{P_r}{P_{n_S}}\right)^{n-1}}$$
 (5)

where  $P_r$  is the required axial compressive strength using LRFD or ASD load combinations and  $P_{ns}$  is the cross-section compressive strength.

To consider the additional contribution to stiffness reduction of residual stresses, expressions for  $\tau_b$  for buckling about the major and minor axis were calibrated against the major (x-x) and minor (y-y) axis

tangent flexural stiffness reduction obtained from finite element models of stainless steel welded I-section stub columns with residual stresses. A W8×31 cross-section, divided into n = 1440 monitoring areas (each of area  $A_i$ , distance to centroid in the x and y direction  $y_i$  and  $x_i$ , and tangent stiffness  $E_i$ ), was subjected to pure axial compression. For each axis of buckling (x-x and y-y), the numerical stiffness reduction factor  $\tau_{b,FE}$  was calculated through the summation of the contribution of each element i to the flexural stiffness, as given by Eqs. (6) and (7).

$$\tau_{b,x,FE} = \frac{\sum_{i=1}^{n} E_{t,i} A_i y_i^2}{\sum_{i=1}^{n} E A_i y_i^2}$$
 (6)

$$\tau_{b,y,FE} = \frac{\sum_{i=1}^{n} E_{t,i} A_i x_i^2}{\sum_{i=1}^{n} E_{A_i} x_i^2}$$
 (7)

The proposed stiffness reduction factor  $\tau_b$ , accounting for the combined effects of material nonlinearity and residual stresses, was derived on the basis of Eq. (5), but with the strain hardening exponent n modified to an effective strain hardening exponent  $n_{eff}$  to allow for the influence of residual stresses by calibration against the results of Eqs. (6) and (7) for the different axes of buckling. The proposed expression for  $\tau_b$  is given by Eq. (8) and illustrated in Fig. 3, while the values of the effective strain hardening exponents  $n_{eff}$  are presented in Table 2.

215 
$$\tau_b = \frac{1}{1 + 0.002 n_{eff} \frac{E}{F_V} \left(\frac{P_T}{P_{DS}}\right)^{n_{eff} - 1}}$$
 (8)

The differing values of  $n_{eff}$  for the different buckling axes reflect the fact that the flexural stiffness is

reduced more severely for the minor axis than the major axis due to the more detrimental influence of

the compressive residual stresses at the flange tips, as seen in Fig. 3. In the case of rectangular hollow structural sections (HSS), since the residual stresses are small, the ratio of the tangent flexural stiffness to the initial elastic flexural stiffness can be assumed to equal to  $\tau_{b,m}$  (i.e.  $n_{eff}$  equal to n). To retain the same demarcation between cross-sections as the AISC 370 flexural buckling curves (see Table 4), the stiffness reduction function for welded box sections and round HSS is taken equal to that for I-sections buckling about the major axis.

Since  $n_{eff}$  is a function of n, the varying degrees of roundedness of the stress-strain curves for the different grades of stainless steel (with the typical austenitic grade 304, duplex grade S32101 and ferritic grade 41OS studied herein) is reflected in  $\tau_b$ , as shown in Fig. 4. Alongside the proposed stiffness reduction factors, the carbon steel stiffness reduction factor, given by Eq. (4), is also presented in Fig. 4. It can be seen that, unlike in AISC 360 (AISC, 2016b), the stiffness reduction for stainless steel

commences from the onset of loading. This stems from the stiffness reduction function being based on the Ramberg-Osgood material model, which features a contribution from the nonlinear term  $(0.002(f/F_y)^n)$  in Eq. (1)) at all stress levels, despite the actual material response being purely elastic in the initial stages. Nonetheless, the early onset of stiffness reduction is an accurate reflection of the inherent rounded stress-strain response of stainless steel, exacerbated by the influence of the residual stresses. The greatest reduction at low to moderate axial load levels occurs for austenitic stainless steel, mirroring the low limit of proportionality and the low value of the strain hardening exponent n, resulting in the highest degree of nonlinearity of stress-strain response among the three main families of stainless steel.

In ASCE-8-20 (ASCE, 2021), for the design of cold-formed stainless steel structural members, a single column curve, corresponding to that for the minor axis buckling of I-sections in AISC 370, is provided; the value of  $n_{eff}$  for this case is therefore proposed for inclusion in ASCE-8 (ASCE, 2021), as given in Table 2, and presented in Fig. 5 for the typical grades of stainless steel.

## **Amplified Notional Load Approach**

- Application of the stiffness reduction method is inherently an iterative process; the stiffness reduction factors  $\tau_b$  are calculated at the load level of interest and the results of the subsequent second order analysis (GNA) are only valid at that same load level. An alternative, simpler approach that avoids the need for iteration is to replace the use of  $\tau_b$  factors (i.e. by setting  $\tau_b = 1.0$  for all members) with the application of additional notional horizontal loads ( $H_{ANL}$ ). The enhanced notional loads are designed to account indirectly for the effect of the spread of plasticity and residual stresses on the global response of the structure. However, since the additional notional loads impact the behavior of the full structure, rather than just the heavily loaded members, overly conservative resistance predictions can result when  $P-\Delta$  effects are significant.
- 252 Existing provisions for steel structures
- In AISC 360 (AISC, 2016b), additional notional loads of magnitude 0.001 of the total factored gravity
- loads acting at each story of structural frames are defined.
- 255 Development of new provisions for stainless steel structures

The stiffness reduction factors  $\tau_b$  derived for stainless steel herein are more severe than those for carbon steel, reflecting the earlier initiation of yielding of the material. A commensurate increase in the additional notional horizontal load ( $H_{ANL}$ ) from 0.001 to 0.002 of the total factored gravity load applied at each story of structural frames is therefore proposed for inclusion in both AISC 370 and ASCE-8 for stainless steel design. The appropriateness of this proposal is demonstrated in subsequent sections (see also Tables 7, 9, 11-13 and Figures 6, 8, 11 and 13).

## Stiffness Reduction Factor $\tau_g$

- The general stiffness reduction factor  $\tau_g$  accounts for the reduction in member stiffness due to the development and spread of plasticity; it is applied to all members in the structure by uniformly reducing the Young's and shear moduli. For structures that are governed by elastic buckling, the  $\tau_g$  factor results in design strengths approximately equal to  $\tau_g$  times the elastic stability limit.
- 267 Existing provisions for steel structures
  - In AISC 360, a reduction factor  $\tau_g$  of 0.8 is prescribed to account for the reduction in stiffness due to plasticity. The value of 0.8 was derived from benchmark studies presented by (Surovek-Maleck, 2001; Surovek-Maleck & White, 2004b) considering a 0.9 factor for strong-axis beam-column strength predictions and its multiplication by  $\phi$  (0.9). Note that these studies showed that a value of 0.7 (0.8 $\phi$ ) is required for weak axis bending. For slender members, where  $\tau_b$  is equal to unity, the 0.8 factor results corresponds approximately to the margin of safety implied in the column curves i.e.  $0.8 = 0.9 \times 0.877$  (Deierlein, 2003; Surovek-Maleck & White, 2004a).
- 275 Development of new provisions for stainless steel structures
  - In this study,  $\tau_g$  has been calibrated against benchmark results from the nonlinear shell finite element analysis of a series of stainless steel columns, beams, beam-columns and portal frames, considering different cross-section shapes and a range of slenderness values, axial load-to-bending ratios and column-to-beam stiffness ratios for the frames. Based on an extensive range of comparisons, presented in subsequent sections, a value of  $\tau_g = 0.7$  is proposed, as given in Table 2. Note that a single value of  $\tau_g$ , as employed for carbon steel in AISC 360, is deemed suitable for all grades of stainless steel, with the value of 0.7 being roughly equal to the minimum flexural buckling coefficient  $\beta_2$  (see Table 4) that controls the flexural buckling strength of slender columns.

In ASCE-08 (ASCE, 2021), for the design of cold-formed stainless steel structural members, a stiffness reduction factor  $\tau_g$  equal to 0.9 is recommended, as given in Table 2. The difference between the proposed value of  $\tau_g$  for AISC 370 and ASCE-08 reflects the different cross-section force-moment interaction equation, the different column buckling curves and the different moment capacities between the two codes. Note that while  $\tau_g = 0.9$  is larger than the corresponding value of 0.8 used in AISC 360 for steel, since  $\tau_b$  drops below unity at low axial load levels for stainless steel, unlike the case for steel where  $\tau_b = 1.0$  up to  $P = 0.5P_y$ , the overall stiffness reduction (i.e.  $\tau_g \tau_b$ ) is similar between the two materials for slender members (i.e. low axial load levels).

## DESIGN BY SECOND ORDER ELASTIC ANALYSIS

In design by second order elastic analysis (GNA), the stiffness reduction factors are employed to recognise the influence of plasticity and residual stresses. The resistance of the members must be subsequently verified either by member buckling checks or, if initial bow imperfections are included in the members of the analysed structure, cross-section checks. In all cases, an out-of-plumbness ratio of 1/500 must be either directly modeled or applied as a set of equivalent notional loads of magnitude equal to 0.002 times the total gravity load applied at each story of the structure ( $H_{NL}$ ). In Table 3, four options, referred to as Design Cases 1, 2, 3 and 4 and abbreviated to DC1, DC2, DC3 and DC4, for design by second order elastic analysis (geometrically nonlinear analysis, GNA – DC1, DC2; geometrically nonlinear analysis with imperfections GNIA – DC3, DC4) are detailed. Design Cases 1 and 2 require member checks, while Design Cases 3 and 4 include member imperfections and therefore resistances can be verified with cross-section checks only. To take account of the additional capacity due to strain hardening, Design Case 4 utilizes the continuous strength method given in Appendix 2 of AISC 370 and Section 6 of ASCE-8.

## **Member Buckling Checks**

In Design Cases 1 and 2, flexural buckling is accounted for through member buckling checks and the required compressive strength  $P_c$  is taken as the nominal compressive strength equal to the critical stress  $F_{cr}$  multiplied by the cross-section area A. In this study, the critical stress  $F_{cr}$  has been determined using the revised column curves included in AISC 370 (AISC, 2021), and given by Eqs. (9)-(11):

311 
$$F_{cr} = F_e \quad \text{for} \quad \frac{L}{r} \le \beta_0 \sqrt{\frac{E}{F_y}}$$
 (9)

312 
$$F_{cr} = 1.2 \left( \beta_1 \frac{\left(\frac{F_y}{F_e}\right)^{\alpha}}{F_y} \right) F_y \quad \text{for} \quad \beta_0 \sqrt{\frac{E}{F_y}} < \frac{L}{r} \le 5.62 \sqrt{\frac{E}{F_y}}$$
 (10)

313 
$$F_{cr} = \beta_2 F_e \quad \text{for} \quad \frac{L}{r} > 5.62 \sqrt{\frac{E}{F_y}}$$
 (11)

- where  $F_y$  is the yield stress, E is the modulus of elasticity,  $F_e$  is the elastic buckling stress given by Eq.
- 315 (12):

$$F_e = \frac{\pi^2 E}{(L/r)^2} \tag{12}$$

- where L is the effective member length, equal to the laterally unbraced length of the member multiplied
- by the effective length factor K, r is the radius of gyration, and  $\alpha$ ,  $\beta_0$ ,  $\beta_1$  and  $\beta_2$  are the flexural buckling
- 319 coefficients, as defined in Table 4 (Meza, Baddoo & Gardner, 2021). Note that the effective length for
- flexural buckling of all members is taken as the unbraced length herein i.e. K = 1 (AISC, 2021).
- 321 Unlike in AISC 360, these curves take account of the varying influence of residual stresses by
- differentiating between the different axes of buckling and cross-section shapes, in a similar manner to
- 323 EN 1993-1-4 (EN 1993-1-4:2006 + A1:, 2015; Afshan et al., 2015). Additionally, the curves include a
- plateau, as defined by Eq. (9), for members with low slenderness L/r; this recognises that the strength
- of short stainless steel members exceed the yield load as a result of strain hardening.
- 326 In ASCE-8, a single flexural buckling curve is given for all cross-section shapes. The curve is the same
- 327 as that given in AISC 370 for the minor axis flexural buckling of I-section members but with an
- 328 allowance for capacities in excess of the yield load for members with low slenderness (i.e. members
- 329 satisfying  $L/r \le \beta_0 \sqrt{E/F_{\nu}}$ ).
- 330 The flexural strength of members should be calculated considering the limit state of yielding, local
- buckling and lateral-torsional buckling. For the in-plane bending of beams with compact cross-sections,
- only the limit state of yielding needs to be considered and the nominal flexural strength  $M_n$  is given as
- 333  $F_{\nu}Z$ , where Z is the plastic section modulus about the axis of bending. Note that stainless steel exhibits
- substantial levels of strain hardening; in strength governed cases capacities can far exceed the plastic
- moment capacity  $M_p$ . This benefit is captured in the continuous strength method, which features in the
- provisions of both AISC 370 and ASCE-8, as discussed in the following section.

For combined loading, the nonlinear interaction curve given by Eqs. (13) and (14), is employed in both AISC 360 (AISC, 2016b) and 370 (AISC, 2021), while in ASCE-8 (ASCE, 2021) the linear interaction curve given by Eq. (15) is used.

340 
$$\frac{P_r}{P_n} + \frac{8}{9} \frac{M_r}{M_n} \le 1.0 \quad \text{for} \quad \frac{P_r}{P_n} \ge 0.2$$
 (13)

$$\frac{P_r}{2P_n} + \frac{M_r}{M_n} \le 1.0 \quad \text{for} \quad \frac{P_r}{P_n} < 0.2$$
 (14)

$$\frac{P_r}{P_n} + \frac{M_r}{M_n} \le 1.0 \tag{15}$$

- 343 where  $P_r$  and  $M_r$  are the required compressive and flexural strengths, respectively, and  $P_n$  and  $M_n$  are the nominal compressive and flexural strengths, respectively.
- For Design Cases 1 and 2, for the example case of members with compact cross-sections, the resistances
- are therefore verified (according to AISC 370 design) using Eqs. (16) and (17).

$$\frac{P_r}{F_{cr}A} + \frac{8}{9} \frac{M_r}{F_{yZ}} \le 1.0 \quad \text{for} \quad \frac{P_r}{F_{cr}A} \ge 0.2$$
 (16)

348 
$$\frac{P_r}{2F_{cr}A} + \frac{M_r}{F_{\nu}Z} \le 1.0 \quad \text{for} \quad \frac{P_r}{F_{cr}A} < 0.2$$
 (17)

Since the influence of the spread of plasticity and residual stresses are accounted for through stiffness reduction and the influence of out-of-plumbness on the structural response is considered through direct modeling or by the application of notional horizontal loads in a second order analysis, unbraced member lengths are used in the member checks (Deierlein, 2003; Kucukler, Gardner & Macorini, 2014).

## **Cross-section Checks**

If member bow imperfections are included in the structural model, member instability is directly captured in the second order analysis and only cross-section strength checks are required to verify the capacity of the structure. This method is set out in Appendix 1 of both AISC 360 (AISC, 2016b) and 370 (AISC, 2021). The cross-section strength check is performed using Eqs. (13) and (14), but with the nominal compressive strength of the member  $P_n$  taken as the cross-section compressive strength  $F_yA$ , where A is the cross-section area, or as  $F_yA_e$  for members with slender elements, where  $A_e$  is the effective area of the cross-section; the resulting cross-section interaction curve is given by Eqs. (18) and (19) for the case of compact cross-sections. This method is referred to herein as Design Case 3 – see Table 3.

$$\frac{P_r}{F_v A} + \frac{8}{9} \frac{M_r}{F_v Z} \le 1.0 \quad \text{for} \quad \frac{P_r}{F_v} \ge 0.2 \tag{18}$$

$$\frac{P_r}{2F_y A} + \frac{M_r}{F_y Z} \le 1.0 \quad \text{for} \quad \frac{P_r}{F_y A} < 0.2 \tag{19}$$

Note that in AISC 360 (AISC, 2016b), the use of additional notional loads in place of stiffness reduction through  $\tau_b$  is not permitted with the method described in this sub-section; the same restriction is applied in AISC 370 (AISC, 2021).

# 367 Continuous strength method

The continuous strength method (CSM) is a deformation based design approach that enables a rational exploitation of the spread of plasticity, strain hardening and element interaction in the design of stainless steel cross-sections (Afshan & Gardner, 2013; Gardner, 2008). The method is set out in Appendix 2 of AISC 370 (and is also included for the calculation of flexural strength in Chapter 6 of ASCE-8), and can be used for the verification of members with initial bow imperfections through second order elastic analysis (GNIA) plus CSM cross-section checks. This method of design is referred to as Design Case 4 – see Table 3. The same interaction equations (i.e. Eqs. (13) and (14)) apply, but with the CSM cross-section resistances in compression  $P_{n,csm}$  and bending  $M_{n,csm}$  used in place of  $P_n$  and  $M_n$  to give:

$$\frac{P_r}{P_{n,csm}} + \frac{8}{9} \frac{M_r}{M_{n,csm}} \le 1.0 \quad \text{for} \quad \frac{P_r}{P_{n,csm}} \ge 0.2$$
 (20)

377 
$$\frac{P_r}{2P_{n,csm}} + \frac{M_r}{M_{n,csm}} \le 1.0 \quad \text{for} \quad \frac{P_r}{P_{n,csm}} < 0.2$$
 (21)

378 where  $P_{n,csm}$  is given by:

379 
$$P_{n,csm} = \frac{\varepsilon_{csm}}{\varepsilon_y} F_y A_g \quad \text{for} \quad \frac{\varepsilon_{csm}}{\varepsilon_y} < 1.0$$
 (22)

380 
$$P_{n,csm} = F_{csm} A_g \quad \text{for} \quad \frac{\varepsilon_{csm}}{\varepsilon_{\nu}} \ge 1.0$$
 (23)

and  $M_{n,csm}$  is given by:

382 
$$M_{n,csm} = \frac{\varepsilon_{csm}}{\varepsilon_y} M_y$$
 for  $\frac{\varepsilon_{csm}}{\varepsilon_y} < 1.0$  (24)

383 
$$M_{n,csm} = M_p \left( 1 + \frac{E_{sh}}{E} \frac{S}{Z} \left( \frac{\varepsilon_{csm}}{\varepsilon_{\gamma}} - 1 \right) - \left( 1 - \frac{S}{Z} \right) / \left( \frac{\varepsilon_{csm}}{\varepsilon_{\gamma}} \right)^{\alpha} \right) \quad \text{for} \quad \frac{\varepsilon_{csm}}{\varepsilon_{\gamma}} \ge 1.0$$
 (25)

where  $F_{csm}$  is the CSM design stress, as given by Eq. (26),  $\varepsilon_y$  is the yield strain equal to  $F_y/E$ ,  $E_{sh}$  is the strain hardening modulus, as given by Eq. (27), where  $C_2$  is equal to 0.16 for austenitic and duplex stainless steel and 0.45 for ferritic stainless steel,  $M_y$  is the elastic moment capacity,  $M_p$  is the plastic moment capacity, S is the elastic section modulus, S is the plastic section modulus, and S is the ultimate

tensile strain, estimated as  $\varepsilon_u = 1 - F_y/F_u$  for austenitic and duplex stainless steel and as  $\varepsilon_u = 0.6(1 - F_y/F_u)$  for ferritic stainless steel.

390 
$$F_{csm} = F_y + E_{sh} \varepsilon_y \left( \frac{\varepsilon_{csm}}{\varepsilon_y} - 1 \right) \quad \text{for} \quad \frac{\varepsilon_{csm}}{\varepsilon_y} \ge 1.0$$
 (26)

$$E_{sh} = \frac{F_u - F_y}{C_2 \varepsilon_u - \varepsilon_y} \tag{27}$$

The ratio  $\varepsilon_{csm}/\varepsilon_y$  defines the maximum strain that the cross-section can tolerate  $\varepsilon_{csm}$  as a multiple of the yield strain, and is obtained from Gardner, Wang & Liew (2011):

394 
$$\frac{\varepsilon_{csm}}{\varepsilon_y} = \frac{0.25}{\lambda_l^{3.6}} \le \min\left(\Lambda, \frac{C_1 \varepsilon_u}{\varepsilon_y}\right) \quad \text{for} \quad \lambda_l \le 0.68$$
 (28)

395 
$$\frac{\varepsilon_{csm}}{\varepsilon_{y}} = \left(1 - \frac{0.222}{\lambda_{l}^{1.05}}\right) \frac{1}{\lambda_{l}^{1.05}} \quad \text{for } 0.68 < \lambda_{l} \le 1.6$$
 (29)

Eqs. (28) and (29) are applicable to non-slender and slender cross-sections, respectively, where  $\lambda_l$  (denoted  $\bar{\lambda}_{p,cs}$  in prEN 1993-1-4 (prEN 1993-1-4, 2020)) is the cross-sectional slenderness,  $C_1$  is equal to 0.1 for austenitic and duplex stainless steels and 0.4 for ferritic stainless steels (Afshan & Gardner, 2013; Bock, Gardner & Real, 2015), and  $\Lambda$  (denoted  $\Omega$  in EN 1993-1-4 (prEN 1993-1-4, 2020)), is a project specific design parameter defining the maximum allowable level of plastic deformation (Fieber, Gardner & Macorini, 2019a). For design by elastic analysis with stiffness reduction,  $\Lambda$  is equal to 5.

## DESIGN BY SECOND ORDER INELASTIC ANALYSIS

The most accurate representation of the behavior of a structure, leading to the most accurate design method, is achieved through the use of second order inelastic analysis – also referred to as geometrically and materially nonlinear analysis with imperfections (GMNIA). In this approach, the influence of the material nonlinearity on the structural response is directly modeled through the definition of the full stress-strain curve of the material in the second order analysis. Plastic hinges do not provide an accurate reflection of the gradual spread of plasticity seen in stainless steel structures. It is therefore necessary to account for the zones of plasticity by directly modeling the nonlinear material stress-strain response in a plastic zone, also known as distributed plasticity or fibre, analysis (Walport *et al.*, 2019). A new method for the design of stainless steel structures by second order inelastic analysis with imperfections (GMNIA), performed using beam finite element analysis is included in Appendix 1 of AISC 370 (AISC, 2021; Walport, Gardner & Nethercot, 2021). This corresponds to Design Case 5 (DC5) in Table 3. In this design method, accurate material modeling is ensured through use of the two-stage Ramberg-

Osgood expression, while cross-section strength checks are replaced by the application of strain limits. The strain limits depend on the slenderness of the cross-section. Consequently, cross-section slenderness dependent levels of spread of plasticity, moment redistribution and strain hardening can be exploited, in a consistent and rational manner enabling accurate predictions of the resistance of structural systems. The strain limits are taken from the CSM, as given by Eqs. (30) and (31), where f is the maximum stress level in the cross-section and n is the strain hardening exponent of the Ramberg–Osgood material model. Note that these Equations differ from the CSM base curve given by Eqs. (28) and (29) to account for the difference between the bilinear and rounded stress-strain curves. Also, a stricter limit is placed on the maximum value of  $\lambda_l$  (1.0 instead of 1.6) for system level design by second order inelastic analysis (GMNIA).

425 
$$\frac{\varepsilon_{csm}}{\varepsilon_{\nu}} = \frac{0.25}{\lambda_{l}^{3.6}} + \frac{0.002}{\varepsilon_{\nu}} \quad \text{but } \frac{\varepsilon_{csm}}{\varepsilon_{\nu}} \le \Lambda \text{ for } \lambda_{l} \le 0.68$$
 (30)

426 
$$\frac{\varepsilon_{csm}}{\varepsilon_{y}} = \left(1 - \frac{0.222}{\lambda_{l}^{1.05}}\right) \frac{1}{\lambda_{l}^{1.05}} + \frac{0.002(f/f_{y})^{n}}{\varepsilon_{y}} \quad \text{for } 0.68 < \lambda_{l} \le 1.0$$
 (31)

To allow for the beneficial influence of moment gradients, the maximum compressive strains output from the second order inelastic analysis (GMNIA) at each cross-section are averaged over the elastic local buckling half-wavelength  $L_{el}$ , denoted  $L_{b,cs}$  in prEN 1993-1-4 (prEN 1993-1-4, 2020), (Fieber, Gardner & Macorini, 2019a; Walport, Gardner & Nethercot, 2021). The elastic local buckling half-wavelength of the cross-section  $L_{el}$  may be obtained numerically or using the simplified expressions given in Fieber, Gardner & Macorini (2019b) – the magnitude of the elastic local buckling half-wavelength will normally be in the region of the cross-section plate widths. The value of  $L_{el}$  also defines the maximum length of the beam elements to be utilized in the analysis.

Initial geometric imperfections and residual stresses must be considered in the analysis and can be

modeled as either (1) a member bow imperfection of magnitude L/1000, where L is the member length, plus residual stresses, or (2) an equivalent member imperfection that accounts for the combined influence of geometric imperfections and residual stress, as given by Eq. (32), where  $e_0$  is the bow imperfection magnitude,  $\alpha_{eq}$  is the imperfection factor (prEN 1993-1-4, 2020), the values of which are given in Table 5 for common cases, and  $\beta = 1/150$  (Walport, Gardner & Nethercot, 2020).

441 
$$\frac{e_0}{L} = \alpha_{eq}\beta \quad \text{but} \quad \frac{e_0}{L} \ge \frac{1}{1000}$$
 (32)

Through this method of design by second order inelastic analysis with imperfections (GMNIA), failure of a system occurs either at the load level at which the CSM strain limit is reached, or, in stability dominated cases, at the load level at which the analysis reaches a peak (Walport, Gardner & Nethercot, 2021).

#### ASSESSMENT OF PROPOSALS FOR MEMBER DESIGN

The accuracy and reliability of the developed recommendations for the design of stainless steel columns, beams and beam-columns is assessed in this section with respect to the benchmark shell FE ultimate loads determined using GMNIA.

In this section, the results of the elastic and inelastic design methods, as outlined in Table 3, are

#### Results

446

447

448

449

450

451

452

453

454

455

456

457

458

459

460

461

462

463

464

465

466

467

468

469

470

compared against benchmark shell FE results for austenitic, duplex and ferritic stainless steel columns, beams and beam-columns. Note that Design Case 2 is not considered in this section as this only relates to analyses at system level. Design Cases 1, 3 and 4 incorporate the developed stiffness reduction factors combined with elastic analysis, while Design Case 5 utilizes inelastic analysis. These are summarised as follows - DC1: GNA +  $\tau_g$  +  $\tau_b$  + member check, DC3: GNIA +  $\tau_g$  +  $\tau_b$  + cross-section check, DC4: GNIA +  $\tau_g$  +  $\tau_b$  + cross-section check + CSM end points and DC5: GMNIA (equivalent imperfections) + CSM strain limits. Table 6 presents the results from the austenitic, duplex and ferritic stainless steel W8×31 and SHS8×8×3/8 cross-section beam-columns considered in this study. Five member slenderness values L/r (20, 40, 80, 120 and 160), where L is the member length and  $r = \sqrt{I/A}$  is the radius of gyration with I being the moment of inertia (second moment of area) and A the cross-sectional area, and three bending moment distributions (BMD) along the member length (BMD 1:  $\psi = 1$ , BMD 2:  $\psi = 0$ , BMD 3:  $\psi = -1$ 0.5), achieved by changing the ratio of applied end moments  $\psi = M_2/M_1$ , where  $M_1$  and  $M_2$  are the applied end moments, were considered. Note that for the duplex stainless steel members, which have higher strengths than other grades and hence are more strongly influenced by buckling effects for a given geometry, only the practical L/r ratios of 20, 40 and 80 were considered. It can be seen that for all grades of stainless steel, the proposed stiffness reduction factors  $\tau_b$  and  $\tau_g$  result in generally safe sided average capacity predictions compared with the benchmark shell FE results (ranging between 27% on the safe side to 6% on the unsafe side).

Fig. 6 shows a comparison between the capacity predictions of the austenitic stainless steel W-section columns, beams and beam-columns subjected to major axis bending obtained using the four design approaches and the benchmark shell FE results. The results are presented in terms of the radial error versus the radial angle, as defined in Fig. 7, where  $R_{FE}$  and  $R_d$  are the radial distances measured from the origin to the data points in M-N space determined from the benchmark FE model and the considered design approach, respectively. Values of radial error larger than unity indicate safe-sided predictions. A radial angle of 0° corresponds to pure bending while a radial angle of 90° corresponds to pure compression. The level of scatter in the predictions (either side of the mean) of Design Cases 1 to 4 is similar to that obtained using the equivalent rules for carbon steel structures (Surovek-Maleck & White, 2004b; Ziemian & Wang, 2019). The scatter is related, in part, to the use of a uniform  $\tau_g$  and the lack of consideration given to the influence of the shape of the bending moment diagram on the development of the plasticity (Kucukler, Gardner & Macorini, 2016); this can be seen in the results presented in Table 6 and Fig. 6, which become increasingly conservative with increasing bending moment gradient i.e transitioning from BMD 1 to 3. Additionally, while the significant strain hardening effects associated with stainless steel are fully captured through accurate material modeling in the benchmark shell FE results, they are essentially disregarded in Design Cases 1-3 and partially reflected through the use of the CSM end points in Design Case 4. From Fig. 6, it can be seen that when the radial angle is between  $0^{\circ}$  and  $50^{\circ}$ , there are a number of capacity predictions on the unsafe side. This is because, for members subjected to high levels of bending, particularly those of stocky proportions, the real degree of stiffness reduction is greater than that obtained using the proposed design approach, but applying more severe stiffness reduction (i.e. a lower value of  $\tau_g$ ) would render the capacity predictions of slender members and those dominated by compression very conservative. A balance has therefore been struck, with  $\tau_g$  = 0.7 for AISC 370 and  $\tau_g$  = 0.9 for ASCE-8, the appropriateness of which is demonstrated in the reliability analyses presented in the following sub-section (see also Table 6). Design Case 5, in which the full nonlinear stress-strain response is explicitly modeled and the influence of moment gradients is captured through strain averaging provides very accurate and consistent results for all three loading arrangements. Note, in particular, that the standard deviation of the radial error is considerably lower for DC5 than all cases of design by second order elastic analysis (GNA/GNIA), ranging between 0.03 and 0.07, compared with 0.04 and 0.21 for DC1-4 – see Table 6.

471

472

473

474

475

476

477

478

479

480

481

482

483

484

485

486

487

488

489

490

491

492

493

494

495

496

497

498

## **Reliability Analysis**

The safety of the proposed structural design provisions are assessed in this sub-section. Values of the resistance factor  $\phi$  have been calculated from Eq. (33) for each dataset, based on a target reliability index  $\beta$  equal to 2.6 and a dead-to-live load ratio of 1:3 (SCI, 2013; Bartlett *et al.*, 2003; Lin, Yu & Galambos, 1992). The recommended value for the resistance factor  $\phi$  is 0.9 and this is therefore taken as the target value in the present study.

$$\phi = \frac{1.481 M_m F_m P_m}{\exp(\beta \sqrt{V_R^2 + V_Q^2})}$$
 (33)

In Eq. (33),  $M_m$ ,  $F_m$  and  $P_m$  are the mean values of the random variables associated with material properties, cross-section geometry and design rule assumptions, respectively, and  $V_R$  and  $V_Q$  are the coefficient of variation of the load effect Q and resistance R, respectively. The coefficient of variation of the resistance  $V_R$  is calculated from Eq. (34), where  $V_M$ ,  $V_F$  and  $V_P$  are the coefficients of variation associated with the uncertainties in material properties, fabrication and design rule assumptions, respectively. The parameters considered in this study are given in Table 7 (Afshan *et al.*, 2015; Baddoo, Meza & Gardner, 2020).

$$V_R = \sqrt{V_M^2 + V_F^2 + V_P^2} \tag{34}$$

The calculated required  $\phi$  factors are presented in Table 6, where it can be seen that all values are greater than the value of 0.9 included in AISC 370, and therefore the target reliability is achieved. In some cases, the  $\phi$  factors are well in excess of 0.9 (with a maximum  $\phi$  value of 1.24), suggesting overconservatism. However, as well as achieving desirable  $\phi$  factor values, weight was also given to ensuring that the mean capacity predictions for the different groups considered were not too much on the unsafe side (i.e. with an average  $\varepsilon$  ratio below unity) and similarly, that capacities of individual members were not excessively over-predicted. It should also be noted that stainless steels have high over-strength factors (see Table 7) which, in the AISC reliability analysis framework, uniformly benefit all members, regardless of their slenderness and the applied loading, while in reality, the benefit of overstrength dissipates with increasing slenderness as instability dominates. Overall, the attained  $\phi$  factors are similar to those achieved in the reliability assessment of the other design provisions in AISC 370 (AISC, 2021), as outlined in DG27 (SCI, 2013). A resistance factor of 0.9 is therefore recommended.

#### APPLICATION OF METHOD TO STRUCTURAL FRAMES

In this section, the accuracy of all five design cases, including Design Case 2 (GNIA +  $\tau_g$  +  $H_{ANL}$  + member check), for the in-plane design of stainless steel frames is assessed. As previously outlined, an alternative to applying the stiffness reduction factors  $\tau_b$ , which is an iterative process, is to impose additional notional horizontal loads ( $H_{ANL}$ ) of magnitude 0.002 of the total factored gravity load applied at that story of the structure. Fig. 8 shows a comparison of the results of a one bay fixed based austenitic stainless steel ( $F_v = 205 \text{ N/mm}^2$ ,  $E = 193000 \text{ N/mm}^2$ ) portal frame obtained from (1) benchmark shell FE GMNIA and (2) Design case 2 i.e. second order elastic analysis (GNA) with no member imperfections modeled, a stiffness reduction of  $\tau_g$  applied to all members, a notional horizontal load of magnitude 0.002 times the vertical load (to represent out-of-plumbness), an additional notional horizontal load ( $H_{ANL}$ ) of the same magnitude and member checks, in which  $P_{ns}$  and  $M_p$  correspond to the column buckling resistance and major axis plastic bending moment resistance of the columns, respectively. The ratio of the column height  $L_c$  to beam length  $L_b$  was fixed at 1:3, resulting in a ratio of the flexural stiffness of the columns to that of the beams of  $G_R = (I_c/L_c)/(I_b/L_b) \approx 1.0$ , while three column lengths were modeled to achieve a range of member slenderness values L/r. It can be seen in Fig. 8 that the stiffness reduction method with additional notional loads  $(H_{ANL})$  results in safe sided predictions in all cases. The level of conservatism increases as the bending moment increases. This is the result of two limitations to the approach: (1) the additional notional load  $(H_{ANL})$  does not consider the variation in axial load level between members, as captured in  $\tau_b$ , and therefore effectively applies to members on the basis of their contribution, through their elastic stiffnesses, to the lateral stability of the frame and (2) the member check limits the bending capacity to the plastic moment capacity  $M_p$ , while the benchmark shell FE model captures the beneficial influence of strain hardening.

## **Vogel Frame**

528

529

530

531

532

533

534

535

536

537

538

539

540

541

542

543

544

545

546

547

548

549

550

551

552

553

554

555

556

557

In this sub-section, the second order elastic (DC1 to DC4 – GNA/GNIA) and inelastic (DC5 – GMNIA) design methods presented herein are applied to the six-story Vogel frame (Vogel, 1985), as shown in Fig. 9, with austenitic stainless steel material properties ( $E = 193000 \text{ N/mm}^2$ ,  $F_y = 205 \text{ N/mm}^2$ ,  $F_u = 515 \text{ N/mm}^2$ , n = 7). The benchmark frame response was determined using second order inelastic analysis with imperfections (GMNIA - L/1000 + residual stresses) using beam finite elements. Beam elements were deemed to be acceptable in the benchmark model since the behavior of the Vogel frame is controlled by overall stability, rather than cross-section strength, and a very similar result would

therefore be expected from a shell FE simulation. Fig. 10 shows the load-deformation path of the Vogel frame; for validation of the modeling approach, a GMNIA of the Vogel frame was also carried out using the original steel material properties ( $E = 205000 \text{ N/mm}^2$ ,  $F_v = 235 \text{ N/mm}^2$ ) and plotted alongside the original response presented by Vogel (Vogel, 1985) – a close match can be observed in Fig. 10. The ultimate design load factors for the Vogel (Vogel, 1985) frame  $\alpha_{DC}$ , calculated as the load level for which the utilisation ratio of the critical member reaches unity for the different design cases (DC1-5), along with benchmark ultimate load factor obtained from GMNIA, are presented in Table 8 and shown in Fig. 11. The  $\alpha_{DC}$  values were determined through iteration for Design Cases 1, 3 and 4, with the stiffness reduction factors recalculated considering the first-order member forces at the load factor  $\alpha_{DC}$ . The capacity predictions for Design Cases 1 to 4 are safe sided and are of similar accuracy to those determined for the equivalent frame in carbon steel by Kucukler, Gardner & Macorini (2016) – average predicted-to-FE capacity ratios of 0.99 to 1.07 compared with 1.02 and 1.06 for the direct analysis method (equivalent to DC1) and notional load method (equivalent to DC2), respectively, for carbon steel. The behavior of the frame is best represented by DC5 since all material and geometric nonlinearities are explicitly modeled, leading to the most accurate prediction of both the distribution of internal forces and moments and structural capacity. Note that the load-deformation path of DC5 differs from the benchmark response due to the use of equivalent geometric imperfections in DC5 (Eq. (32)) instead of the explicit modeling of both geometric imperfections (L/1000) and residual stresses in the benchmark model. The stiffness reduction factors  $\tau_b$  for Design Cases 1-4 at the ultimate system load (i.e. when the critical member had a utilisation equal to unity) for each member in the Vogel frame are presented in Table 9. It can be seen that the middle columns of each story have the lowest stiffness reduction factors, representing the highest level of plasticity. Note that  $\tau_b$  is only applied to the flexural stiffnesses (i.e. by reducing the second moments of areas) of the columns while  $\tau_g = 0.7$  is applied uniformly to all members through the reduction of the Young's modulus E and shear modulus G. As well as the ultimate design load, it is important to consider the accuracy of the prediction of the distribution of forces and moments within the frame. Table 10 presents a comparison of the maximum normalised bending moments within the members of the Vogel frame determined at the ultimate system loads for the five design cases considered. The maximum bending moment in each member at the ultimate system load  $M_{DC}$  is presented normalised by the plastic moment capacity  $M_p$  (i.e.  $M_{DC}/M_p$ ) of

558

559

560

561

562

563

564

565

566

567

568

569

570

571

572

573

574

575

576

577

578

579

580

581

582

583

584

585

586

the member, as well as by the corresponding bending moment obtained from the benchmark GMNIA  $M_{GMNIA}$  (i.e.  $M_{DC}/M_{GMNIA}$ ). The bending moments are generally well predicted, with the largest discrepancies arising in members with relatively low bending moments at failure. For example, in DC1, the maximum  $M_{DC}/M_{GMNIA}$  value of 1.23 occurs in member C26 which has a  $M_{DC}/M_p$  value of 0.09, while the minimum  $M_{DC}/M_{GMNIA}$  value of 0.89 occurs in member C24, which has a  $M_{DC}/M_p$  value of 0.24. These two members correspond to the least heavily loaded members in bending and therefore the accuracy of the moment predictions is deemed reasonable.

For all design cases, C21 is the critical member that governs failure. For DC1, DC3, DC4 and DC5 the bending moments in this critical member are well predicted with  $M_{DC}/M_{GMNIA}$  values of 0.96, 1.00, 1.05 and 1.04, respectively. As observed in Kucukler, Gardner & Macorini (2016), DC2 does not consider the influence of the differential rates of plasticity in the structure on the distribution of internal forces and moments and therefore results in the least accurate predictions of ultimate load and distribution of forces/moments when compared with the benchmark results. The additional notional load ( $H_{ANL}$ ), used

in DC2 to mimic the influence of plasticity and residual stresses accounted for in  $\tau_b$ , impacts the

behavior of the full frame, rather than just the highly loaded members, and overestimates the maximum

bending moment resisted by the critical member (C21) by 26% in comparison to GMNIA.

## **Asymmetric Frame**

In this sub-section, the second order elastic (GNA/GNIA) and inelastic (GMNIA) design methods presented herein are applied to the multistory asymmetric frame shown in Fig. 12, with ferritic stainless steel material properties ( $E = 200000 \text{ N/mm}^2$ ,  $F_y = 205 \text{ N/mm}^2$ ,  $F_u = 415 \text{ N/mm}^2$ , n = 14). The benchmark results were obtained by means of geometrically and materially nonlinear analysis with imperfections (L/1000 + residual stresses) using shell finite elements.

The ultimate load factors of the frame  $\alpha_{DC}$ , calculated as the load level for which the utilisation rate of the critical member becomes equal to unity, for the different design cases (DC1-5), as well as the ultimate load factor obtained from the benchmark shell FE model are presented in Table 11 and shown in Fig. 13. The  $\alpha_{DC}$  values were determined through iteration for Design Cases 1, 3 and 4, with the stiffness reduction factors recalculated considering the first order member forces at the load factor  $\alpha_{DC}$ . However, note that in the considered frame, the axial loads in the members were all less than  $P/P_{ns} = 0.2$  and consequently  $\tau_b = 1.0$  in all cases (see Fig. 4c); this explains the similar design predictions for the four elastic design options (DC1-4). The capacity predictions for all design cases are safe sided. The

behavior of the frame is best represented in DC5 since all material and geometric nonlinearities are explicitly modeled, leading to the most accurate prediction of both the distribution of internal forces and moments and structural capacity.

## SUMMARY OF DESIGN PROPOSALS AND WORKED EXAMPLES

618

619

620

621

622

623

624

625

626

627

628

629

630

631

632

633

634

635

636

637

638

639

640

641

642

643

644

645

646

For the design of stainless steel members and structures by second order elastic analysis (GNA/GNIA), the stiffnesses (flexural, axial, torsional) of all members must be uniformly reduced by the general stiffness reduction factor  $\tau_g$  (equal to 0.7 in AISC 370 and 0.9 in ASCE-8), as given in Table 2, and the flexural stiffness of the members contributing to the stability of the structure must be reduced by a further stiffness reduction factor  $\tau_b$ , as given by Eq. (8). Alternatively to the use of  $\tau_b$ , an additional notional load  $(H_{ANL})$  of 0.002 of the total factored gravity load applied at each story may be imposed. In all cases, a notional load  $(H_{NL})$  equal to 0.002 of the total factored gravity load acting at each story to represent the effects of frame out-of-plumbness must be imposed. Buckling checks should be performed to verify the stability of individual members, unless member imperfections are modeled, in which case, only cross-section checks are required. The cross-section checks may be conducted using the CSM, with  $\Lambda = 5$  for this application of the method. For the design of stainless steel members and structures by second order inelastic analysis (GMNIA) with strain limits, the influence of the material nonlinearity on the structural response is directly modeled through the definition of the full stress-strain curve of the material. Initial geometric imperfections and residual stresses may be either individually modeled or their combined effect may be considered through the use of equivalent geometric imperfections. Cross-section failure may be defined in beam finite element models through the application of the CSM strain limits, as given by Eqs. (30) and (31). To allow for the beneficial influence of moment gradients, the maximum compressive strains output from the second order inelastic analysis (GMNIA) at each cross-section may be averaged over the elastic local buckling half-wavelength  $L_{el}$ . Failure of a system is defined either at the load level at which the CSM strain limit is reached, or, in stability dominated cases, at the load level at which the analysis reaches a peak, whichever occurs first. Two worked examples are presented in this section to illustrate the application of the proposed approach of design by second order elastic analysis (GNA/GNIA) with stiffness reduction for stainless steel structures. Worked Example 1 considers an austenitic stainless steel W6×16 beam-column subjected

to combined compression and major axis bending, as shown in Fig. 14, while Worked Example 2 considers a two-story duplex stainless steel portal frame, as shown in Fig. 15.

# Worked Example 1

649

650

651

652

653

654

655

656

657

658

659

Worked Example 1 considers, using Design Case 1, a laterally-restrained austenitic grade 304 stainless steel ( $F_y = 205 \text{ N/mm}^2$ ,  $F_u = 515 \text{ N/mm}^2$ ,  $E = 193000 \text{ N/mm}^2$ ) W6×16 member with a length L = 3810 mm subjected to a major axis bending moment  $M_a = 20.6 \text{ kNm}$  and an axial compression  $N_a = 141.3 \text{ kN}$ , as shown in Fig. 14. The material and geometric properties are included in Fig. 14. Considering the width-to-thickness ratios of the cross-section elements, both the flange and web are compact when the cross-section is under flexure ( $b/t \le 0.41\sqrt{E/F_y}$  and  $h/t_w \le 2.54\sqrt{E/F_y}$ ) and nonslender under axial compression ( $b/t \le 0.41\sqrt{E/F_y}$  and  $h/t_w \le 1.24\sqrt{E/F_y}$ ). It is first necessary to calculate the stiffness reduction factors under the applied loading. Next, a second order elastic analysis (GNA) of the member with reduced stiffness is performed and the maximum force and moment in the member is extracted at the applied load level. The capacity of the member is then verified using the member buckling check.

- 660 Stiffness reduction factors
- The material properties for grade 304 stainless steel were taken as  $F_y = 205 \text{ N/mm}^2$ ,  $E = 193000 \text{ N/mm}^2$
- and n = 7. Since the member is subjected to major axis buckling, the corresponding effective strain
- hardening exponent  $n_{eff} = 0.55n = 3.85$  is used. For the applied axial load, the stiffness reduction factor
- 664  $\tau_b$  is calculated as:

$$\tau_b = \frac{1}{1 + 0.002 n_{eff} \frac{E}{F_y} \left(\frac{P}{P_y}\right)^{n_{eff}-1}}$$

$$\tau_b = \frac{1}{1 + 0.002(3.85) \frac{193000}{205} \left(\frac{141.3}{619.8}\right)^{3.85 - 1}} = 0.903$$

- Combined with the general stiffness reduction factor  $\tau_g = 0.7$ , the stiffness of the member must be
- 668 reduced by  $\tau_g \tau_b = 0.632$ .
- 669 Beam FE analysis second order elastic analysis
- The member length L of 3810 mm was discretised into 30 elements and a second order elastic analysis
- 671 (GNA) with stiffness reduction was carried out. Note that a smaller number of elements can be used

- when justified through a mesh convergence study. Fig. 14b shows the resulting bending moment
- diagram at the applied load level. From the analysis, the required compressive and flexural strengths  $P_r$
- 674 = 141.3 kN and  $M_{rx}$  = 24.4 kNm, respectively, were determined.
- 675 Determine available compressive strength
- The nominal compressive strength  $P_n$  must be determined based on the limit state of flexural buckling.
- The member considered has a slenderness ratio L/r = 3810/66.12 = 57.6. Since  $L/r > 0.891\sqrt{E/F_V}$
- and  $L/r \le 5.62\sqrt{E/F_{\nu}}$ , the critical stress  $F_{cr}$  is given by:

679 
$$F_{cr} = 1.2 \left( \beta_1 \left( \left( \frac{F_y}{F_e} \right)^{\alpha} \right) \right) F_y = 1.2 \left( 0.455 \left( \left( \frac{205}{574} \right)^{0.58} \right) \right) 205 = 159 \text{ N/mm}^2$$

- Therefore, the nominal compressive strength  $P_n = AF_{cr} = 482.1$  kN and the available compressive
- strength  $P_c$  is  $\phi_c P_n = 433.9$  kN (LRFD).
- 682 Determine available flexural strength
- For a member bending about the major axis, the limit states of yielding and lateral-torsional buckling
- apply. However, the considered member has adequate restraint to prevent lateral-torsional buckling and
- consequently the limit state of yielding will control. Since the cross-section has compact web and
- flanges, the nominal flexural strength is:

$$M_{nx} = F_{v}Z_{x} = 38.7 \text{ kNm}$$

- Therefore, the available flexural strength  $M_{cx}$  is  $\phi_c M_{nx} = 34.9$  kNm (LRFD).
- 689 Resistance check
- Since  $P_r/P_c \ge 0.2$ , the resistance is assessed using the interaction equation:

$$\frac{P_r}{P_c} + \frac{8}{9} \frac{M_{rx}}{M_{cx}} \le 1.0$$

692 And

$$\frac{141.3}{4339} + \frac{824.4}{9349} = 0.95$$

Therefore, the chosen  $W6 \times 16$  section is adequate.

Note that a similar process is applied for the design of cold-formed members using ASCE-8, but with the following changes: (1) the effective strain hardening value  $n_{eff} = 0.45n$  and  $\tau_g = 0.9$ , (2) the compressive strength would be calculated according to Section 5 of ASCE-8 (incorporating a degree of strain hardening) and (3) the ASCE-8 moment-axial interaction equation i.e. Eq. (19) would be employed.

## Worked Example 2

695

696

697

698

699

- Worked Example 2 considers, using Design Case 3, a two story duplex grade S32101 stainless steel ( $F_{\nu}$
- 702 = 450 N/mm<sup>2</sup>,  $F_u = 650$  N/mm<sup>2</sup>, E = 200000 N/mm<sup>2</sup>) frame, restrained out-of-plane, as shown in Fig.
- 15. The material and geometric properties assumed are included in Fig. 15. Member imperfections are
- modeled with an amplitude of L/1000, and out-of-plumbness is considered through the application of
- notional loads  $(H_{NL})$  equal to 0.002 times the gravity load at each story. Considering the width-to-
- thickness ratios of the HEB 340 cross-section, both the flange and web elements are compact when the
- 707 cross-section is under flexure  $(b/t_f \le 0.41\sqrt{E/F_y})$  and  $h/t_w \le 2.54\sqrt{E/F_y})$  and nonslender under
- axial compression  $(b/t_f \le 0.41\sqrt{E/F_y})$  and  $h/t_w \le 1.24\sqrt{E/F_y}$ . The proposed stiffness reduction
- method is implemented through the following key steps:
- 710 (1) Perform a linear elastic analysis (LA) considering out-of-plumbness.
- 711 (2) Calculate the stiffness reduction factors  $\tau_b$  using Eq. (8) based on the member forces determined
- through the LA for each column in the system.
- 713 (3) Reduce the Young's modulus E and shear modulus G of all members by  $\tau_g$  as well as the flexural
- stiffnesses (i.e. the moments of inertia (second moments of area) about the principal axes) of
- 715 the columns by  $\tau_b$ .
- 716 (4) Perform a geometrically nonlinear analysis (GNIA) considering out-of-plumbness and member
- 717 imperfections.
- 718 (5) Since member imperfections are modeled, carry out cross-section checks using the internal
- member forces obtained from the GNIA. Assess the adequacy of the structure.
- 720 Beam FE analysis first order elastic analysis
- All members were discretised into 30 elements and a first order elastic analysis of the frame was carried
- out. The section forces (SF<sub>i</sub>, where i is the column label) in the columns are extracted as:

- 723  $SF_{C1} = 1648.8 \text{ kN}, SF_{C2} = 1950.4 \text{ kN}, SF_{C3} = 842.3 \text{ kN}, SF_{C4} = 957.1 \text{ kN}$
- 724 Stiffness reduction factors
- The material properties for grade S32101 stainless steel were taken as  $F_y = 450 \text{ N/mm}^2$ , E = 200000
- 726 N/mm<sup>2</sup> and n = 8. Since the members are buckling about the major axis, the corresponding effective
- strain hardening exponent  $n_{eff} = 0.55n = 4.4$  is used. For the applied axial load, the stiffness reduction
- 728 factor  $\tau_b$  is calculated for each column as

729 
$$\tau_b = \frac{1}{1 + 0.002 n_{eff} \frac{E}{F_y} \left(\frac{P}{P_y}\right)^{n_{eff}-1}}$$

- 730 The stiffness reduction factors, calculated for each member of the frame, are given in Table 12.
- 731 Beam FE analysis second order elastic analysis
- The members were discretised into 30 elements, and now a second order elastic analysis (GNIA) with
- stiffness reduction is carried out. From the analysis, the required compressive and flexural strengths,  $P_r$
- and  $M_r$ , respectively, at the critical cross-section of each member is determined, as listed in Table 13.
- 735 Determine available compressive strength
- 736 Since member imperfections are modeled in the analysis, the nominal compressive strength of the
- members  $P_n$  is taken as the cross-section compressive strength  $F_vA$ . Therefore, the nominal compressive
- strength  $P_n$  is equal to 7408.8 kN and the available compressive strength  $P_c$  is  $\phi_c P_n = 6667.9$  kN (LRFD).
- 739 Determine available flexural strength
- 740 For major axis flexure, the limit states of yielding and lateral-torsional buckling apply. However, the
- member has adequate restraint to prevent lateral-torsional buckling and consequently the limit state of
- yielding will control. Since the cross-section has compact web and flanges, the nominal flexural strength
- 743 is:

$$M_{nx} = F_y Z_x = 1043.5 \text{ kNm}$$

- Therefore, the available flexural strength  $M_{cx}$  is  $\phi_c M_{nx} = 939.2$  kNm (LRFD).
- 746 Resistance check

For members C1 and C2,  $P_r/P_c \ge 0.2$  and the resistance is assessed using the following interaction equation:

$$\frac{P_r}{P_c} + \frac{8}{9} \frac{M_{rx}}{M_{cx}} \le 1.0$$

For members C3, C4, B1 and B2,  $P_r/P_c < 0.2$  and the resistance is assessed using the following interaction equation:

$$\frac{P_r}{2P_c} + \frac{M_{rx}}{M_{cx}} \le 1.0$$

- The results of the cross-section checks on the six frame members are presented in Table 14. For all members, the interaction equation is less than unity; therefore, the frame is adequate.
- Note that for structures composed of cold-formed members and designed using ASCE-8, the following
- 756 changes would need to be made: (1) the effective strain hardening value  $n_{eff} = 0.45n$  and  $\tau_g = 0.9$ , (2) the
- 757 compressive strength would be calculated according to Section 5 of ASCE-8 (incorporating a degree of
- strain hardening) and (3) the ASCE-8 moment-axial interaction equation i.e. Eq. (15) would be
- 759 employed.

760

761

762

763

764

765

766

767

768

769

770

771

772

773

774

## CONCLUSIONS

- Stability design rules for stainless steel structures have been established in this paper. For design by second order elastic analysis (also referred to as geometrically nonlinear analysis (GNA) with imperfections (GNIA)), two stiffness reductions factors are defined: (1) a general stiffness reduction factor  $\tau_g$ , to be applied to all member stiffnesses (axial, flexural, torsional) to account for the development and spread of plasticity and (2)  $\tau_b$ , to account for the additional reduction in the flexural stiffness of compression members under increasing axial load due to the effects of yielding and residual stresses. The influence of the varying degree of roundedness of the stress-strain behavior on the level of stiffness reduction for the different grades of stainless steel is reflected in the strain hardening exponent n that features in the Ramberg-Osgood formulation. A value of  $\tau_g = 0.7$  for AISC 370 and  $\tau_g = 0.9$  for ASCE-8 is proposed; the different values for the two specifications reflect the different buckling curves and axial-bending interaction expressions and end-points employed.
- Shell finite element models of the stainless steel members and frames have been developed, validated against experimental results from the literature, and employed to verify the proposed design rules for a wide range of cases. The proposed stiffness reduction factors  $\tau_b$  and  $\tau_g$  result in safe sided average

- 775 capacity predictions compared with the benchmark shell FE results. The level of scatter in the
- 776 predictions is similar to that of the carbon steel rules of AISC 360. Comparisons have also been made
- against the new provisions in AISC 370 for design by second order inelastic analysis (also referred to
- as geometrically and materially nonlinear analysis with imperfections (GMNIA)) with strain limits; this
- 779 represents the most accurate design approach. The reliability of the design proposals has been
- demonstrated through statistical analyses, where it was shown that a resistance factor  $\phi$  of 0.9 can be
- safely adopted.
- The design provisions presented herein are due to be incorporated into the new upcoming AISC 370
- 783 Specification for hot-rolled and welded stainless steel structures and the revised ASCE-8 Specification
- for the design of cold-formed stainless steel structures.

## 785 ACKNOWLEDGEMENTS

- Funding for this investigation was received from the Engineering and Physical Sciences Research
- 787 Council (EPSRC) through the EPSRC Doctoral Prize scheme.

## 788 DATA AVAILABILITY STATEMENT

- 789 Some or all data, models, or code that support the findings of this study are available from the
- 790 corresponding author upon reasonable request.

#### 791 **REFERENCES**

- 792 ABAQUS (2014) *Abaqus CAE User's Manual, Version 6.14*. Pawtucket, USA, Hibbitt, Karlsson & Sorensen, Inc.
- Afshan, S., Francis, P., Baddoo, N.R. & Gardner, L. (2015) Reliability analysis of structural stainless steel design provisions. *Journal of Constructional Steel Research*. 114, 293–304.
- Afshan, S. & Gardner, L. (2013) The continuous strength method for structural stainless steel design. *Thin-Walled Structures*. 68, 42–49.
- 798 AISC (2016a) AISC 303-16 Code of standard practice for steel buildings and bridges. AISC.
- 799 AISC (2016b) AISC 360. Specification for Structural Steel Buildings. AISC.
- 800 AISC (2021) AISC 370. Specification for Structural Stainless Steel Buildings. Draft for public review. 801 AISC.
- 802 AISI (2016) AISI S100-16. North American Specification for the Design of Cold-Formed Steel Structural Members. AISI.
- Arrayago, I., Real, E. & Gardner, L. (2015) Description of stress-strain curves for stainless steel alloys. *Materials and Design*. 87, 540–552.
- ASCE (2021) ASCE-8-21: Specification for the Design of Cold-Formed Stainless Steel Structural
  Members. Draft for public review. ASCE.
- Baddoo, N.R. & Francis, P. (2014) Development of design rules in the AISC Design Guide for structural stainless steel. *Thin-Walled Structures*. 83, 200–208.
- Baddoo, N.R., Meza, F.J. & Gardner, L. (2020) *Proposed overstrength for AISC 370 and ASCE 8*. SCI Report.

- Bartlett, F.M., Dexter, R.J., Graeser, M.D., Jelinek, J.J., et al. (2003) Updating standard shape material properties database for design and reliability. *Engineering Journal, AISC*. 40, 2–14.
- Bock, M., Gardner, L. & Real, E. (2015) Material and local buckling response of ferritic stainless steel sections. *Thin-Walled Structures*. 89, 131–141.
- Bu, Y. & Gardner, L. (2019a) Finite element modelling and design of welded stainless steel I-section columns. *Journal of Constructional Steel Research*. 152, 57–67.
- Bu, Y. & Gardner, L. (2019b) Laser-welded stainless steel I-section beam-columns: Testing, simulation and design. *Engineering Structures*. 179, 23–36.

826

827

832

833

834

835

836

837838

839

840

841

842

843

844

845

846 847

848

849

850

851

- Chan, S.L., Liu, Y.P. & Liu, S.W. (2011) Structural design in the post-effective length era. *Procedia Engineering*. 14, 1005–1012.
- Deierlein, G. (2003) Background and Illustrative Examples on Proposed Direct Analysis Method for Stability Design of Moment Frames. *Report on behalf of AISC TC 10*. 1–17.
- Ellobody, E. & Young, B. (2005) Structural performance of cold-formed high strength stainless steel columns. *Journal of Constructional Steel Research*. 61, 1631–1649.
  - EN 1993-1-4:2006 + A1: (2015) Eurocode 3 Design of steel structures Part 1-4: General rules Supplementary rules for stainless steels. Brussels, CEN.
- 828 EN 1993-1-5 (2009) Eurocode 3 Design of steel structures Part 1-5 : Plated structural elements. 829 Brussels, CEN.
- Fieber, A., Gardner, L. & Macorini, L. (2019a) Design of structural steel members by advanced inelastic analysis with strain limits. *Engineering Structures*. 199, 109624.
  - Fieber, A., Gardner, L. & Macorini, L. (2019b) Formulae for determining elastic local buckling half-wavelengths of structural steel cross-sections. *Journal of Constructional Steel Research*. 159, 493–506.
  - Fieber, A., Gardner, L. & Macorini, L. (2020) Structural steel design using second-order inelastic analysis with strain limits. *Journal of Constructional Steel Research*. 168, 105980.
    - Gardner, L. (2008) The continuous strength method. *Proceedings of the Institution of Civil Engineers Structures and Buildings*. 161 (3), 127–133.
    - Gardner, L. & Nethercot, D.A. (2004) Numerical modeling of stainless steel structural components A consistent approach. *Journal of Structural Engineering ASCE*. 130 (10), 1586–1601.
  - Gardner, L., Wang, F. & Liew, A. (2011) Influence of strain hardening on the behavior and design of steel structures. *International Journal of Structural Stability and Dynamics*. 11 (5), 855–875.
  - Jandera, M., Gardner, L. & Machacek, J. (2008) Residual stresses in cold-rolled stainless steel hollow sections. *Journal of Constructional Steel Research*. 64 (11), 1255–1263.
  - Kucukler, M. & Gardner, L. (2018) Design of laterally restrained web-tapered steel structures through a stiffness reduction method. *Journal of Constructional Steel Research*. 141, 63–76.
  - Kucukler, M. & Gardner, L. (2019) Design of web-tapered steel beams against lateral-torsional buckling through a stiffness reduction method. *Engineering Structures*. 190, 246–261.
  - Kucukler, M., Gardner, L. & Macorini, L. (2014) A stiffness reduction method for the in-plane design of structural steel elements. *Engineering Structures*. 73, 72–84.
  - Kucukler, M., Gardner, L. & Macorini, L. (2016) Development and assessment of a practical stiffness reduction method for the in-plane design of steel frames. *Journal of Constructional Steel Research*. 126, 187–200.
- Kucukler, M., Gardner, L. & Macorini, L. (2015) Flexural-torsional buckling assessment of steel beam-columns through a stiffness reduction method. *Engineering Structures*. 101, 662–676.
- Kucukler, M., Xing, Z. & Gardner, L. (2020) Behaviour and design of stainless steel I-section columns in fire. *Journal of Constructional Steel Research*. 164, 105890.
- 858 Liew, J.Y.R. (1992) Advanced analysis for frame design. Purdue University (PhD Thesis).
- Liew, J.Y.R., White, D.W. & Chen, W.F. (1994) Second-order refined plastic-hinge analysis for frame design. Part I. *Journal of Structural Engineering ASCE*. 119 (11), 3196–3216.
- Lin, S.-H., Yu, W.-W. & Galambos, T.V. (1992) ASCE LRFD method for stainless steel structures. *Journal of Structural Engineering ASCE*. 118 (4), 1056–1070.
- Lui, E.M. & Ge, M. (2005) Analysis and design for stability in the U.S. An overview. *Steel and Composite Structures*. 5 (2), 103–126.
- Meng, X. & Gardner, L. (2020) Behavior and Design of Normal- and High-Strength Steel SHS and RHS Columns. *Journal of Structural Engineering ASCE*. 146 (11), 04020227.

- Meza, F.J., Baddoo, N.R. & Gardner, L. (2021) Development of Flexural Buckling Rules for the New
   AISC Stainless Steel Design Specification. *Proceedings of the 9th European Conference on* Steel and Composite Structures, Eurosteel 2021. Sheffield, UK.
- Mirambell, E. & Real, E. (2000) On the calculation of deflections in structural stainless steel beams: an experimental and numerical investigation. *Journal of Constructional Steel Research*. 54 (1), 109–133.
- Orbison, J.G. (1982) *Nonlinear static analysis of three-dimensional steel frames*. Cornell University (PhD Thesis).
- prEN 1993-1-4 (2020) Eurocode 3 Design of steel structures Part 1-4: General rules Supplementary rules for stainless steels. *CEN*. Draft 2.
- 877 SCI (2013) Steel Design Guide 27: Structural Stainless Steel. Chicago, AISC.

878

879

880

881

882

883

884

885

886 887 888

889

890

892

893

896

897

- Shen, Y. & Chacón, R. (2020a) Flexural stiffness reduction for stainless steel SHS and RHS members prone to local buckling. *Thin-Walled Structures*. 155, 106939.
- Shen, Y. & Chacón, R. (2020b) Geometrically non-linear analysis with stiffness reduction for the stability design of stainless steel structures: Application to members and planar frames. *Thin-Walled Structures*. 148, 106581.
- Surovek-Maleck, A.E. (2001) Second-order inelastic and modified elastic analysis and design evaluation of planar steel frames. Georgia Institute of Technology (PhD Thesis).
- Surovek-Maleck, A.E. & White, D.W. (2004a) Alternative Approaches for Elastic Analysis and Design of Steel Frames. I: Overview. *Journal of Structural Engineering ASCE*. 130 (8), 1186–1196
- Surovek-Maleck, A.E. & White, D.W. (2004b) Alternative approaches for elastic analysis and design of steel frames. II: Verification studies. *Journal of Structural Engineering ASCE*. 130 (8), 1197–1205
- 891 Vogel, U. (1985) Calibrating frames. *Stahlbau*. 10 (54), 295–301.
  - Walport, F., Gardner, L. & Nethercot, D.A. (2021) Design of structural stainless steel members by second order inelastic analysis with CSM strain limits. *Thin-Walled Structures*. 159, 107267.
- Walport, F., Gardner, L. & Nethercot, D.A. (2020) Equivalent bow imperfections for use in design by second order inelastic analysis. *Structures*. 26, 670–685.
  - Walport, F., Gardner, L., Real, E., Arrayago, I., et al. (2019) Effects of material nonlinearity on the global analysis and stability of stainless steel frames. *Journal of Constructional Steel Research*. 152, 173–182.
- Yuan, H.X., Wang, Y.Q., Shi, Y.J. & Gardner, L. (2014) Residual stress distributions in welded stainless steel sections. *Thin-Walled Structures*. 79, 38–51.
- 901 Yura, J.A. (1971) The effective length of columns in unbraced frames. *AISC Engineering Journal*. 8 902 (2), 37–42.
- Ziemian, R.D. & Wang, Y. (2019) Design by advanced analysis 2016 AISC specification. SDSS
   2019 International Colloquium on Stability and Ductility of Steel Structures. Prague, Czech
   Republic.

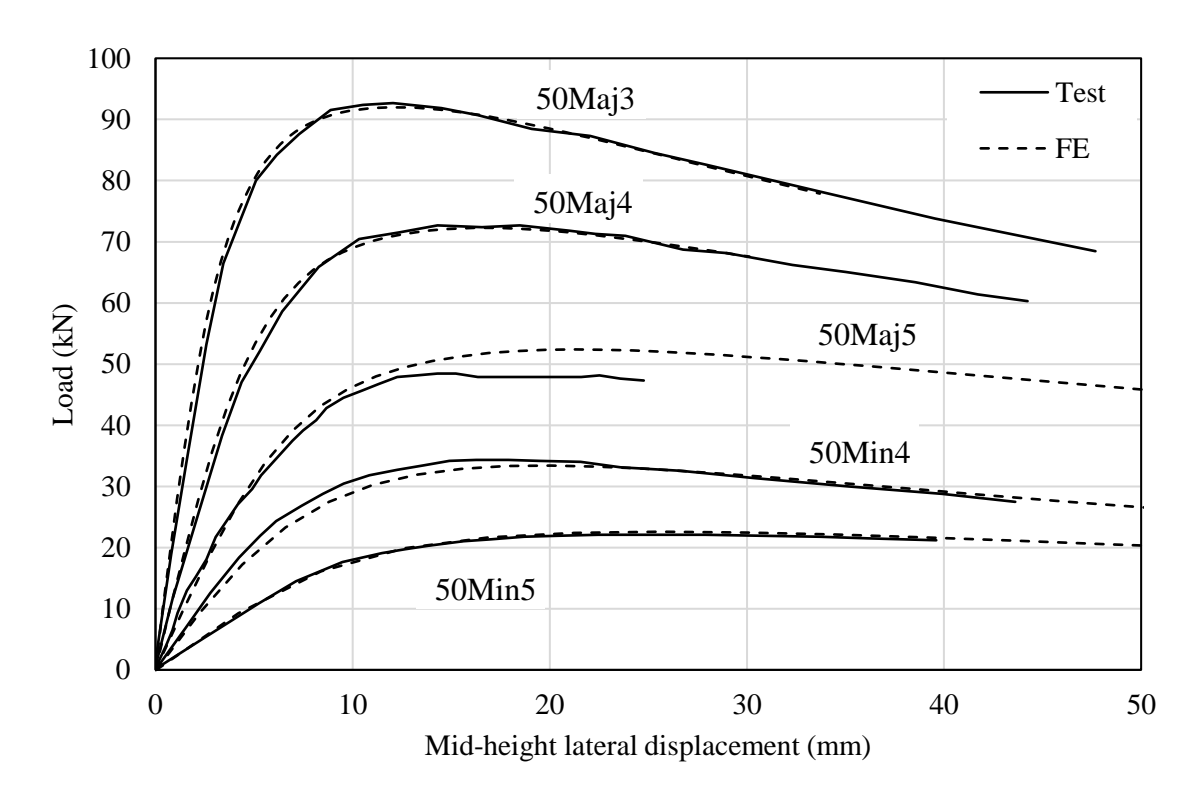
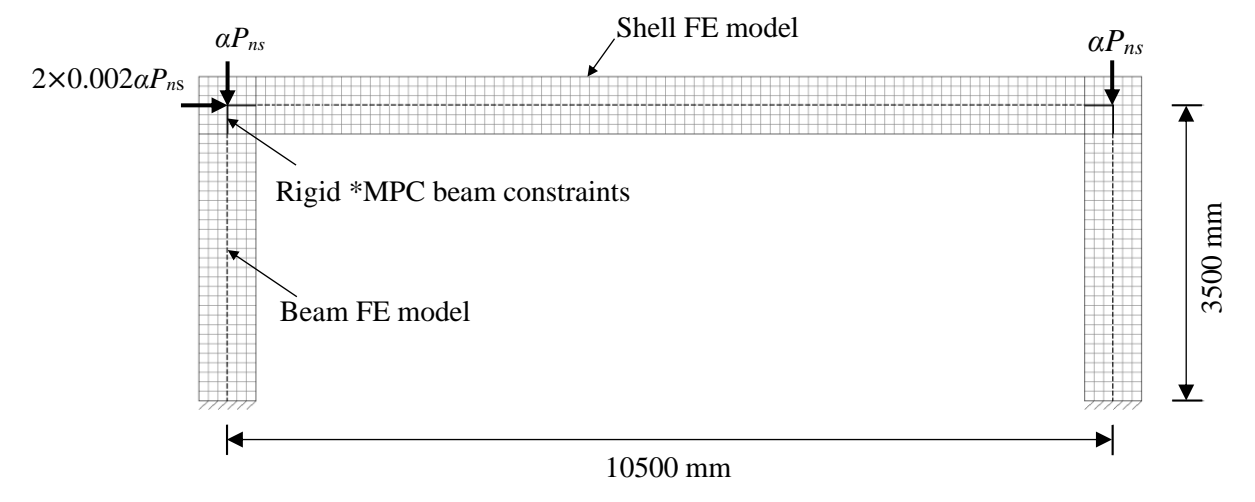


**Fig. 1.** Shell FE model validation against beam-column tests on an austenitic stainless steel I- $50 \times 50 \times 4 \times 4$  cross-section reported by Bu and Gardner (2019b).



(a) Frame modelling with rigid \*MPC beam constraints in beam FE model to represent the rigid beam-to-column connection in the shell FE model

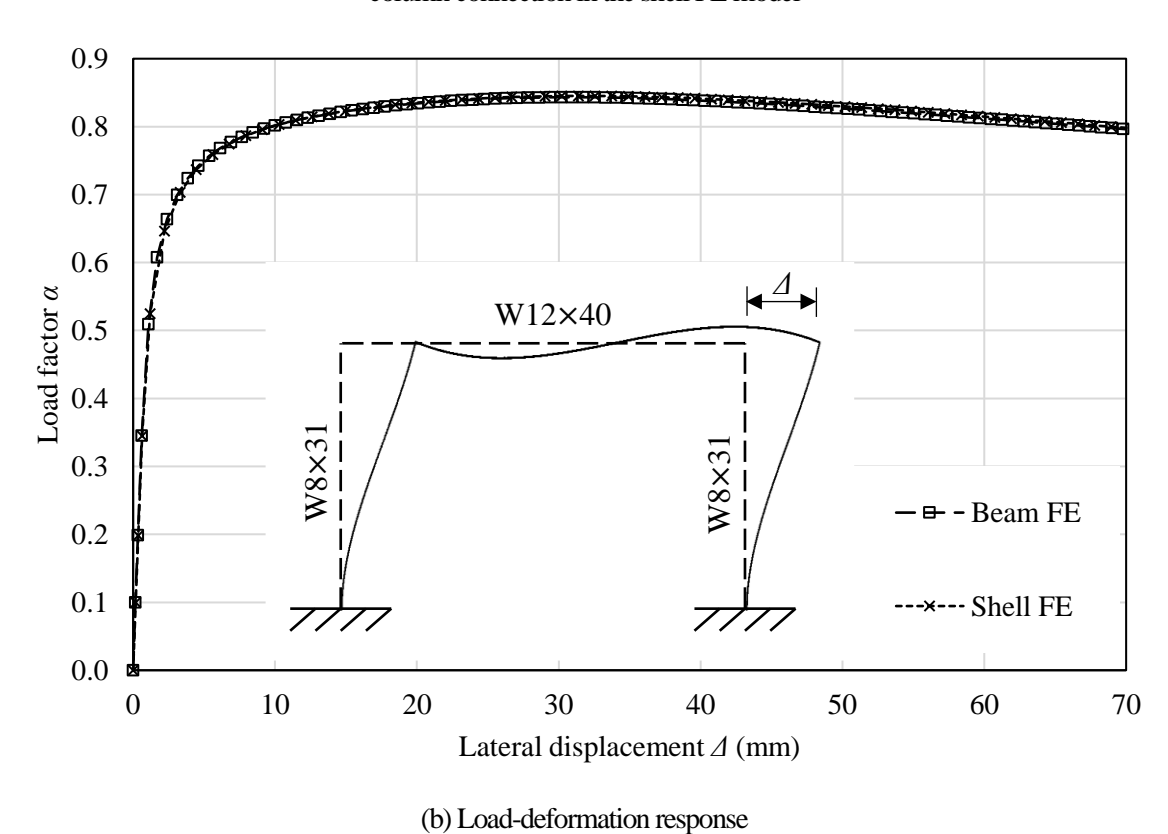
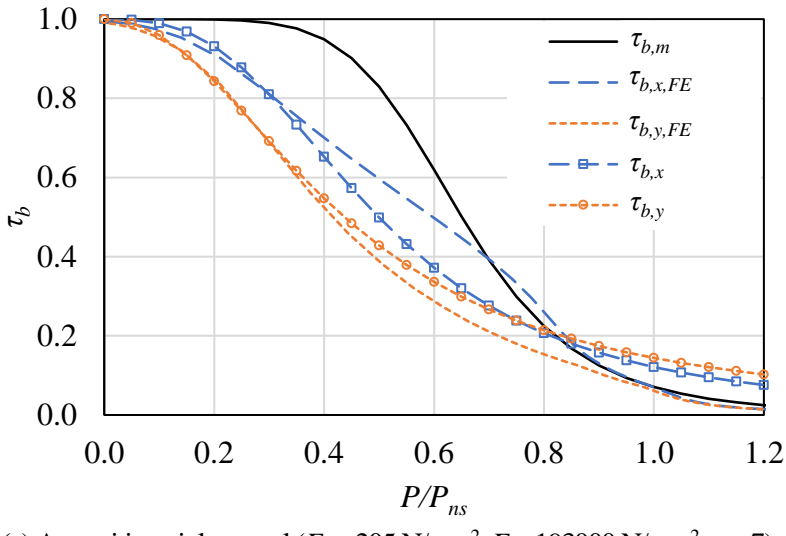
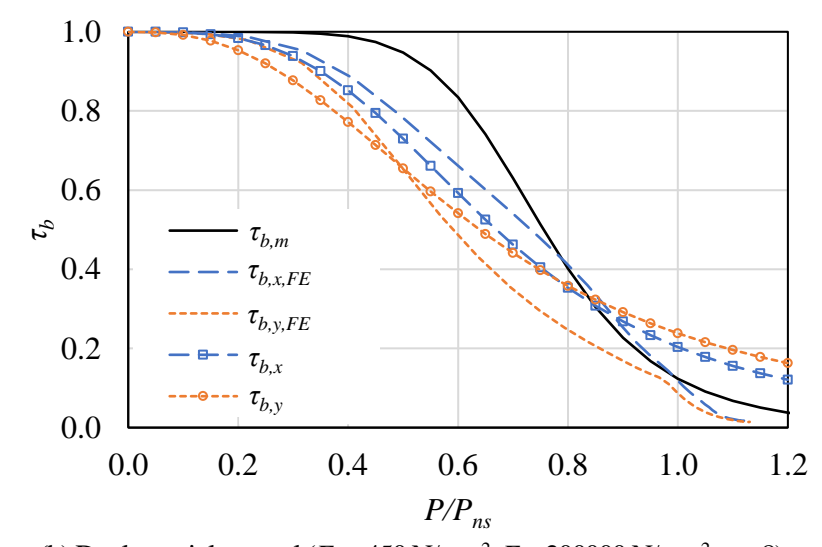


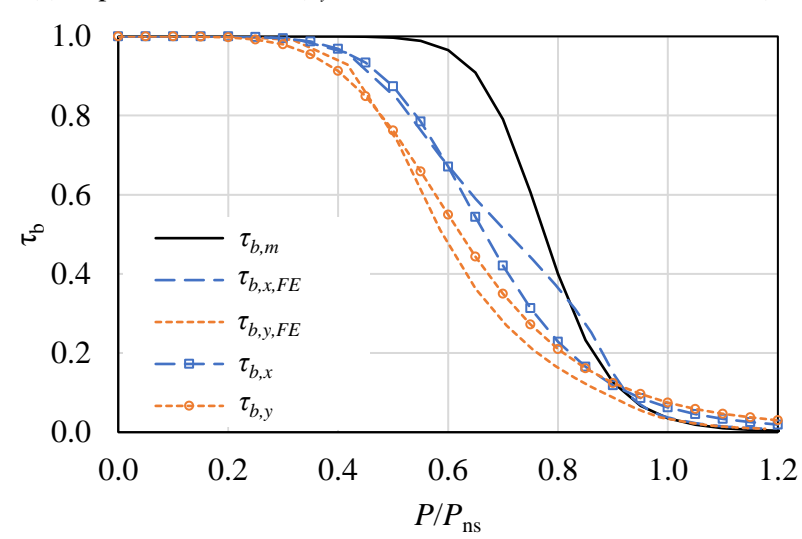
**Fig. 2.** Example austenitic ( $F_y = 205 \text{ N/mm}^2$ ,  $E = 193000 \text{ N/mm}^2$ ) stainless steel fixed based frame to illustrate the finite element (FE) modeling implemented in this study. Note that in both FE models, the same initial imperfections were included (L/1000 + no residual stresses) to allow for direct comparison.



(a) Austenitic stainless steel ( $F_y = 205 \text{ N/mm}^2$ ,  $E = 193000 \text{ N/mm}^2$ , n = 7)

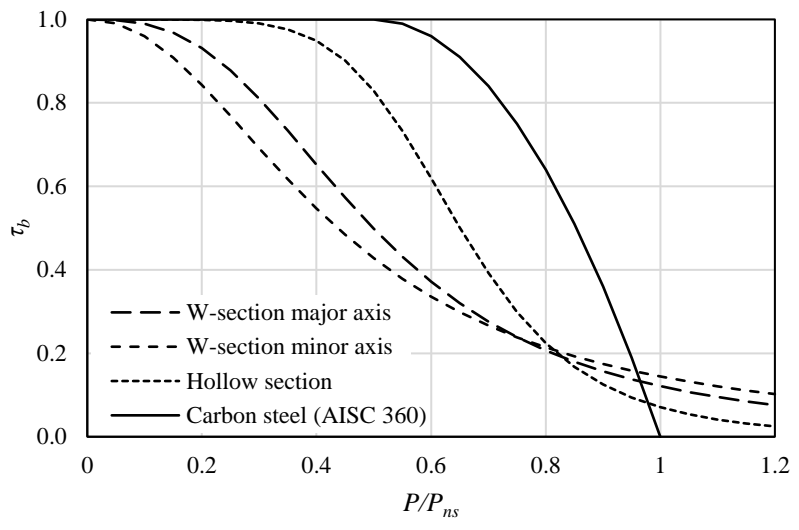


(b) Duplex stainless steel ( $F_y = 450 \text{ N/mm}^2$ ,  $E = 200000 \text{ N/mm}^2$ , n = 8)

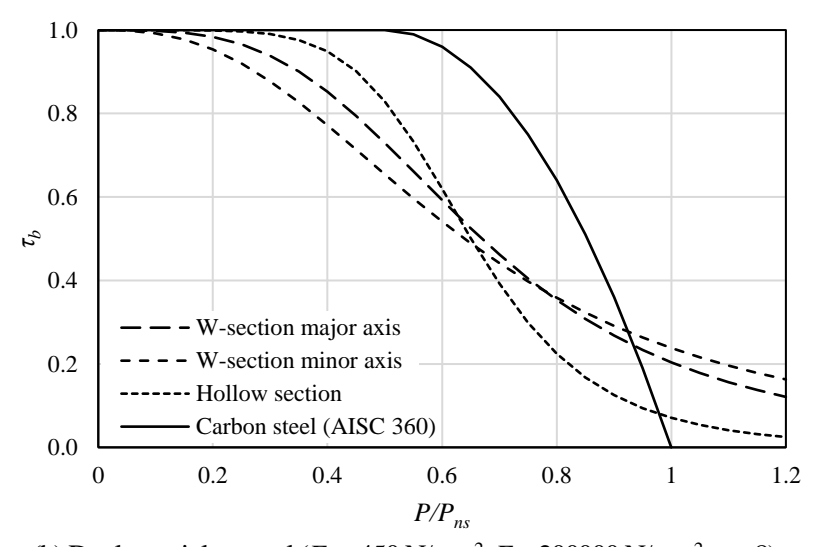


(c) Ferritic stainless steel ( $F_y = 205 \text{ N/mm}^2$ ,  $E = 200000 \text{ N/mm}^2$ , n = 14)

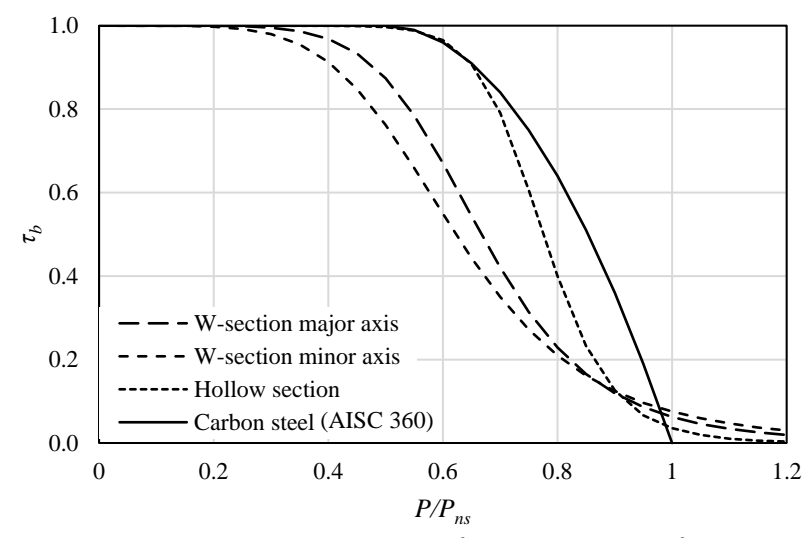
**Fig. 3.** Calibration of effective strain hardening exponents  $n_{eff}$  to derive the stiffness reduction factor  $\tau_b$  to account for the adverse influence of spread of plasticity and residual stresses as a function of the level of axial loading.



(a) Austenitic stainless steel ( $F_y = 205 \text{ N/mm}^2$ ,  $E = 193000 \text{ N/mm}^2$ , n = 7)



(b) Duplex stainless steel ( $F_v = 450 \text{ N/mm}^2$ ,  $E = 200000 \text{ N/mm}^2$ , n = 8)



(c) Ferritic stainless steel ( $F_y = 205 \text{ N/mm}^2$ ,  $E = 200000 \text{ N/mm}^2$ , n = 14)

Fig. 4. AISC 370 stiffness reduction factor  $\tau_b$  for typical austenitic, duplex and ferritic grades of stainless steel. For W-section major axis buckling  $n_{eff} = 0.55n$ , for W-section minor axis buckling  $n_{eff} = 0.45n$ , and for hollow sections  $n_{eff} = n$ . In all cases,  $n_{eff} \ge 2.5$ .

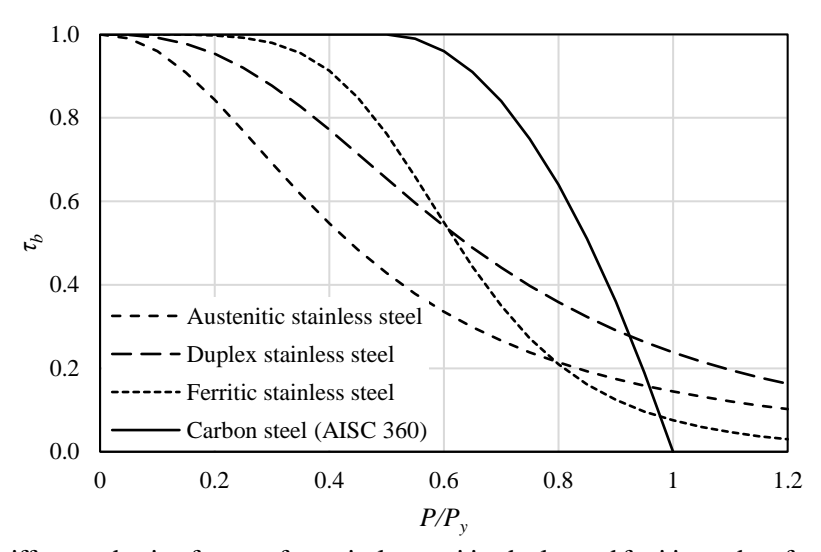


**Fig. 5.** ASCE-08 stiffness reduction factor  $\tau_b$  for typical austenitic, duplex and ferritic grades of stainless steel. For all cases  $n_{\text{eff}} = 0.45n$  (but  $n_{\text{eff}} \ge 2.5$ ).

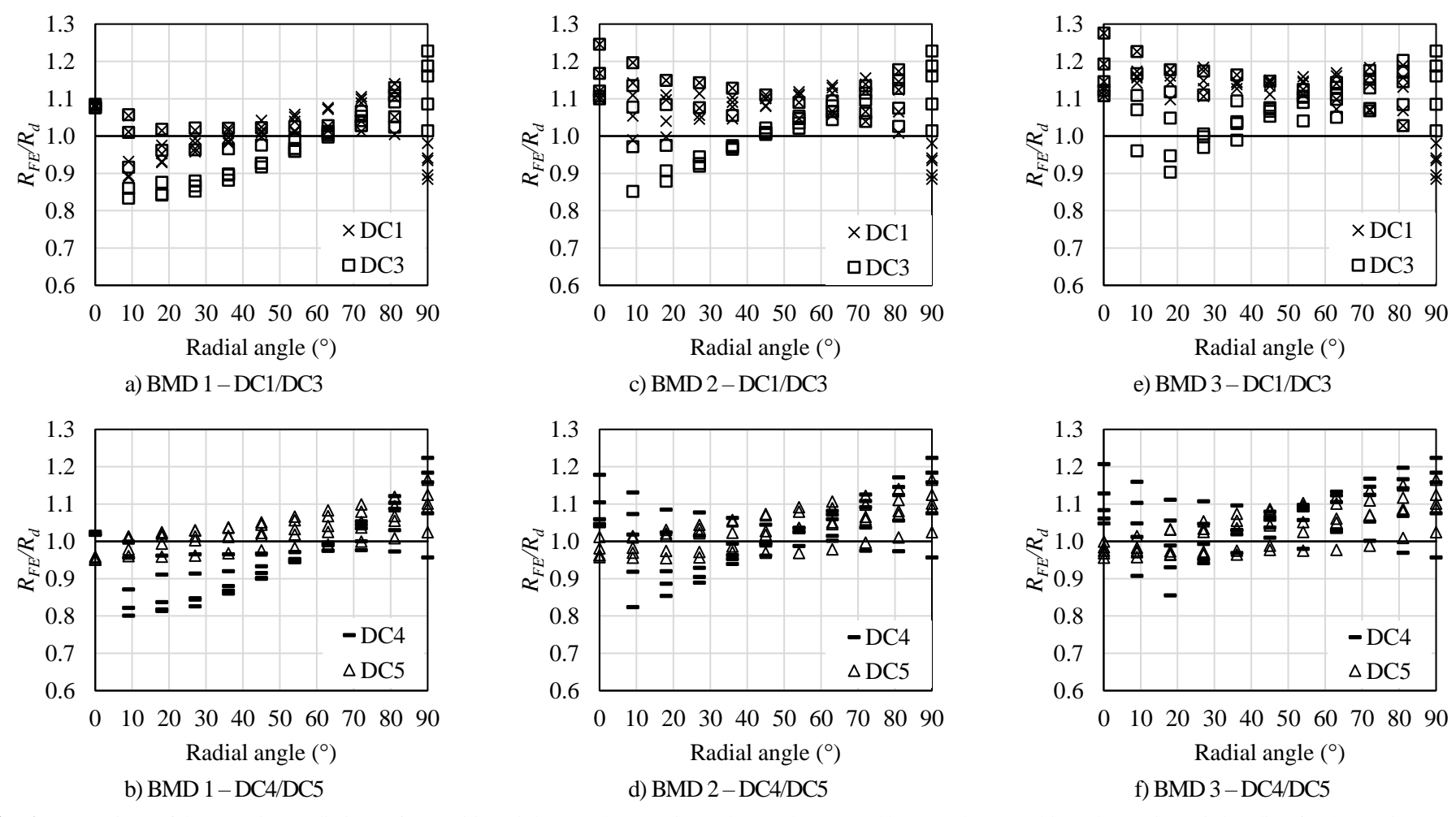


**Fig. 6.** Comparison of the capacity predictions of austenitic stainless steel W-section columns, beams and beam-columns subjected to major axis bending for the Design Cases (DC) 1 (GNA +  $\tau_g$  +  $\tau_b$  + no member imperfections + member check), 3 (GNIA +  $\tau_g$  +  $\tau_b$  + member imperfections (L/1000) + cross-section check), 4 (GNIA +  $\tau_g$  +  $\tau_b$  + member imperfections (equivalent imperfections) + CSM strain limits) against the benchmark shell FE results. Note that a radial angle of equivalent of equivalent are compression.

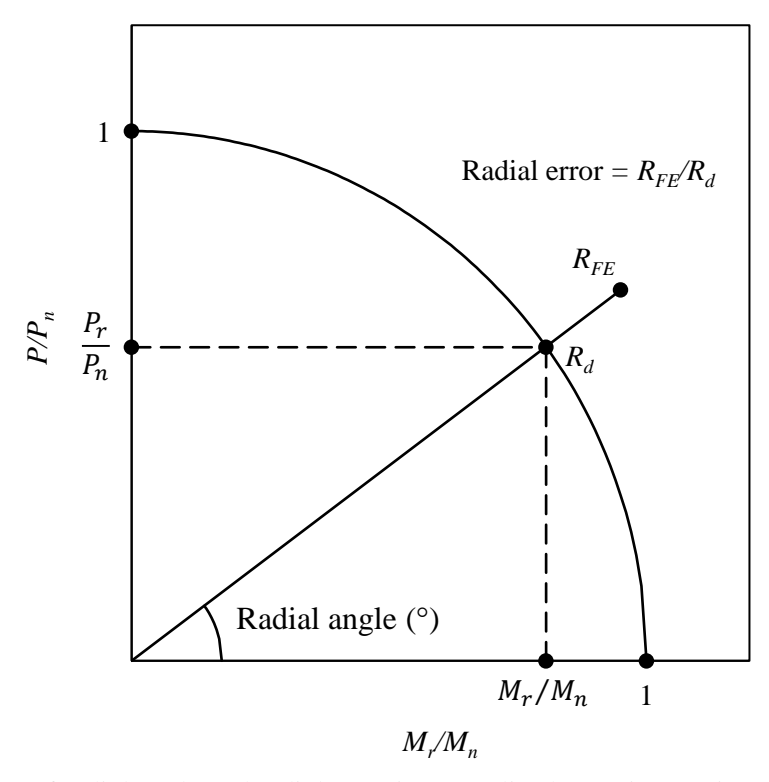


**Fig. 7.** Definition of radial angle and radial error in normalised M-P interaction diagram.

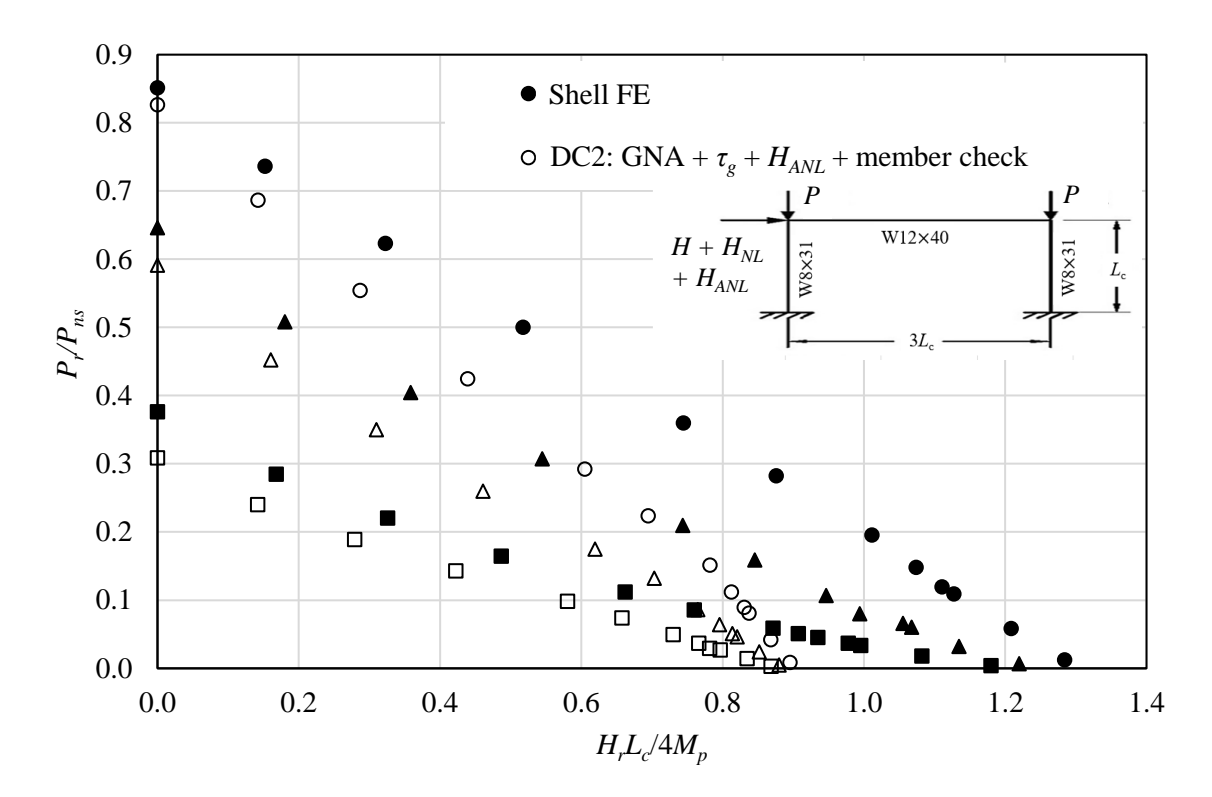


Fig. 8. Comparison of the proposed stiffness reduction method (with  $\tau_g$  and additional notional loads) against shell benchmark FE results for fixed based austenitic stainless steel portal frames considering three values of column slenderness ( $L_c = 3.5 \text{ m} \rightarrow L/r = 40 \text{ (circles)}$ ;  $L_c = 6 \text{ m} \rightarrow L/r = 68 \text{ (triangles)}$ ;  $L_c = 10 \text{ m} \rightarrow L/r = 113 \text{ (squares)}$ ). DC2 – GNA +  $\tau_g$  +  $H_{ANL}$ + no member imperfections + member check.

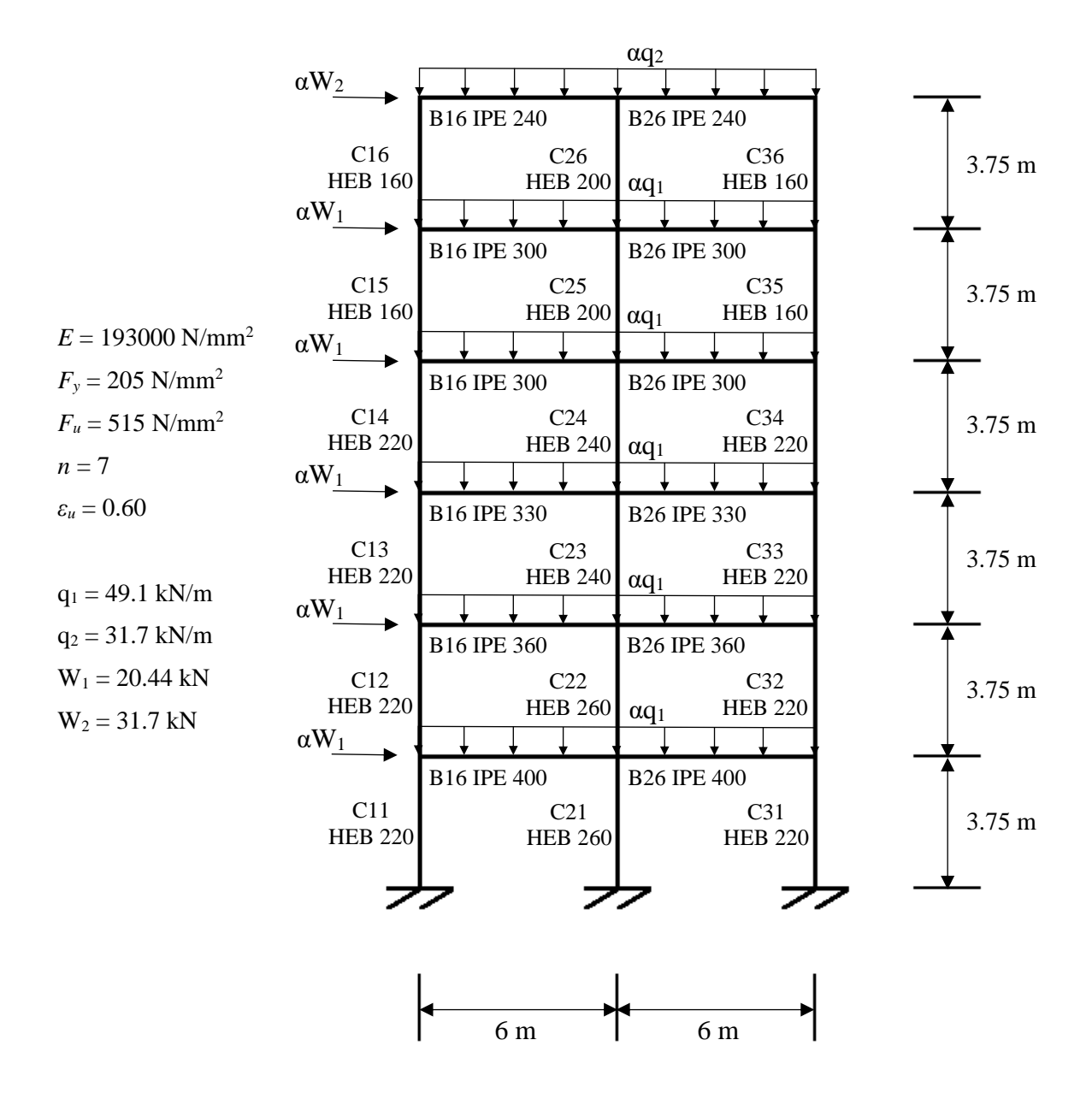
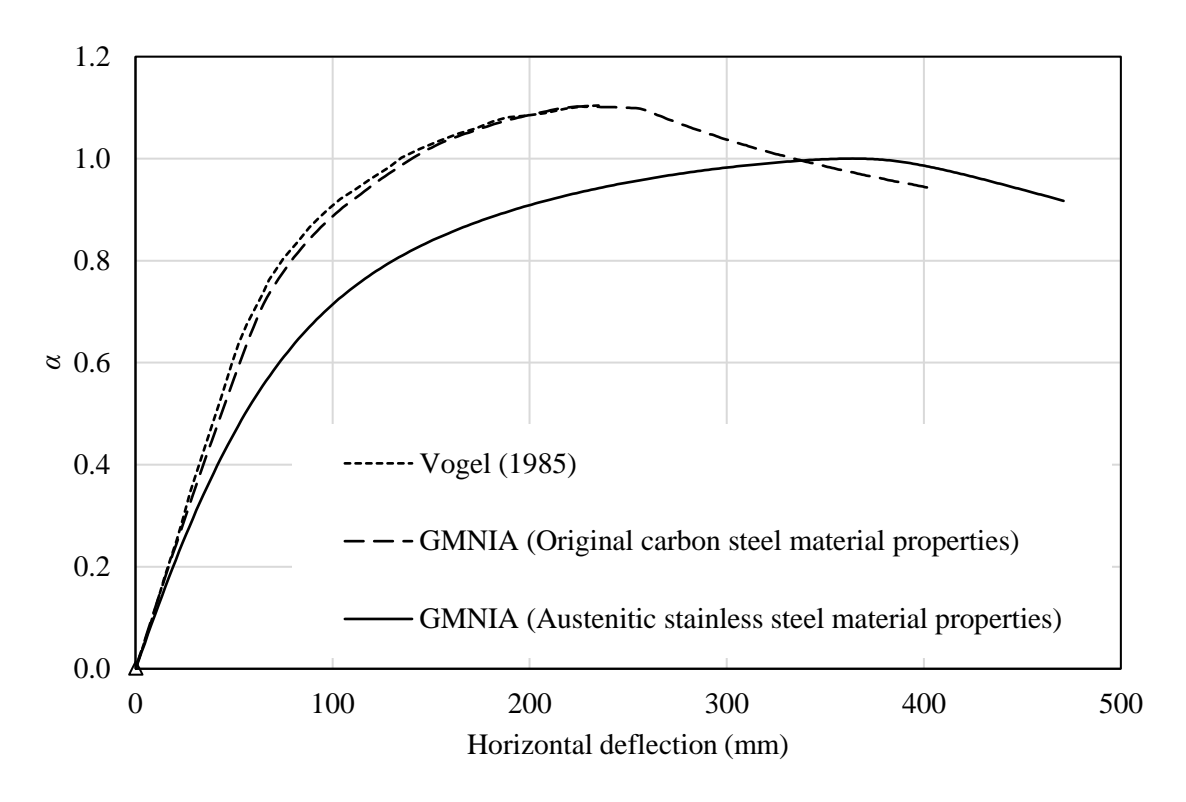
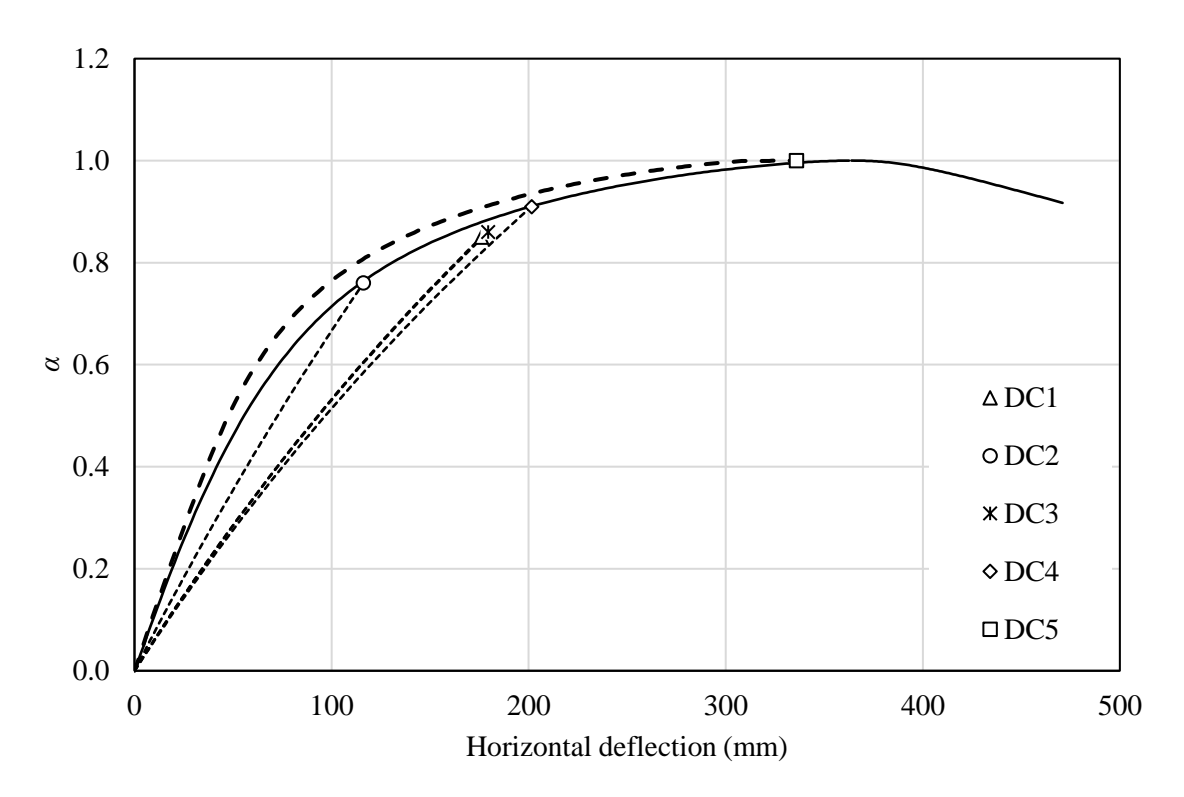


Fig. 9. Geometrical and material properties and loading conditions of the modeled Vogel (1985) frame.



**Fig. 10.** Load-deflection response of Vogel frame modeled with bilinear carbon steel material stress-strain properties and rounded Ramberg-Osgood (R-O) stainless steel material stress-strain properties.



**Fig. 11.** Benchmark GMNIA load-deflection response of Vogel frame and ultimate load factor predictions for five design cases (DC1-5) considered. DC1: GNA +  $\tau_g$  +  $\tau_b$  + no member imperfections + member check, DC2: GNA +  $\tau_g$  +  $H_{ANL}$  + no member imperfections + member check, DC3: GNIA +  $\tau_g$  +  $\tau_b$  + member imperfections (L/1000) + cross-section check, DC4: GNIA +  $\tau_g$  +  $\tau_b$  + member imperfections (L/1000) + cross-section check with CSM end points, and DC5: GMNIA + member imperfections (equivalent imperfection) + CSM strain limits.

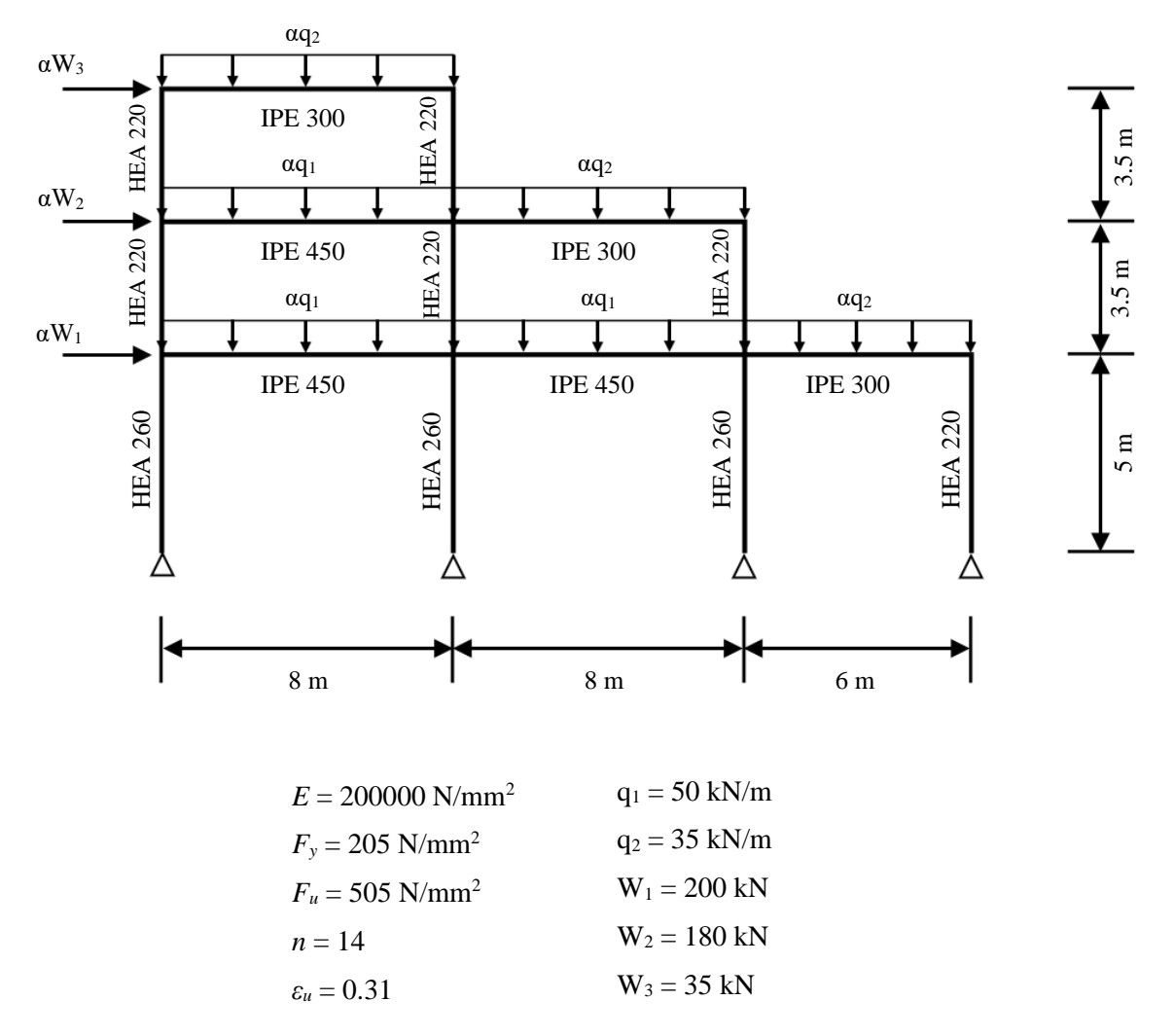


**Fig. 12.** Geometrical and material properties and loading conditions of the modeled ferritic stainless steel multistory asymmetric frame.

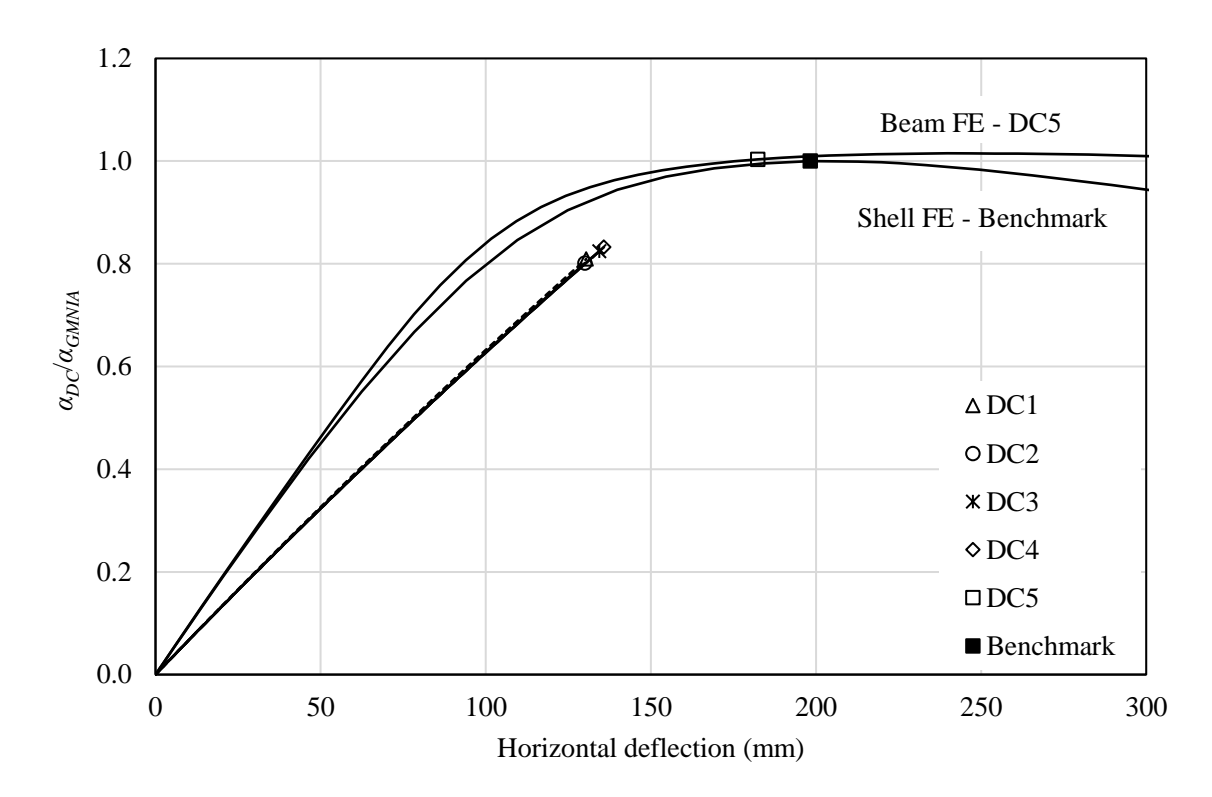


**Fig. 13.** Ultimate load capacity predictions of the multistory asymmetric frame from the stainless steel design cases (DC1-5)  $\alpha_{DC}$  considered normalised by the benchmark capacity  $\alpha_{GMNIA}$ . DC1: GNA +  $\tau_g$  +  $\tau_b$  + no member imperfections + member check, DC2: GNA +  $\tau_g$  +  $H_{ANL}$  + no member imperfections + member check, DC3: GNIA +  $\tau_g$  +  $\tau_b$  + member imperfections (L/1000) + cross-section check, DC4: GNIA +  $\tau_g$  +  $\tau_b$  + member imperfections (L/1000) + cross-section check with CSM end points, and DC5: GMNIA + member imperfections (equivalent imperfection) + CSM strain limits.

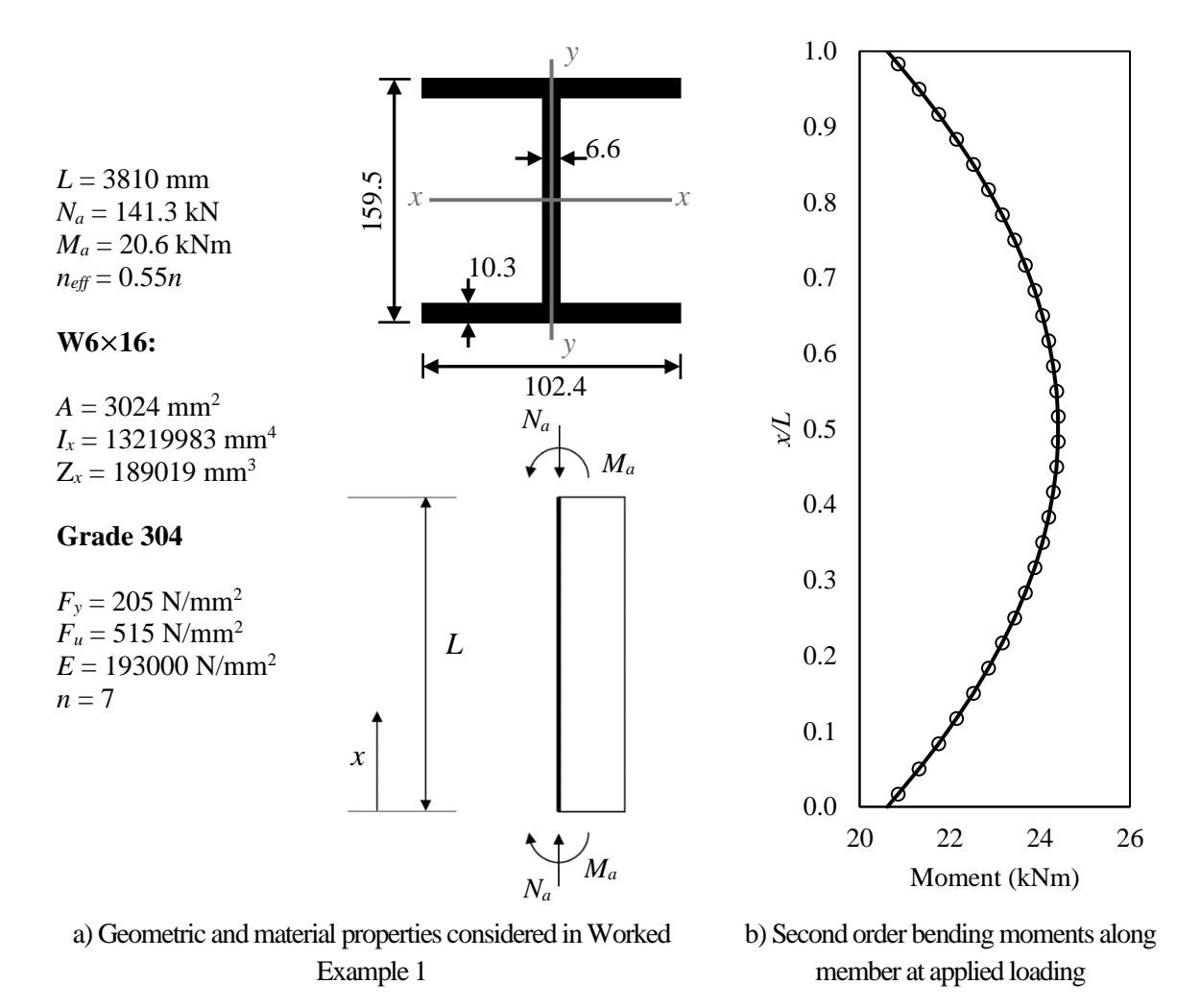


**Fig. 14.** Worked Example 1: W6×16 cross-section under combined compression and major axis bending. All dimensions in mm. Not to scale.

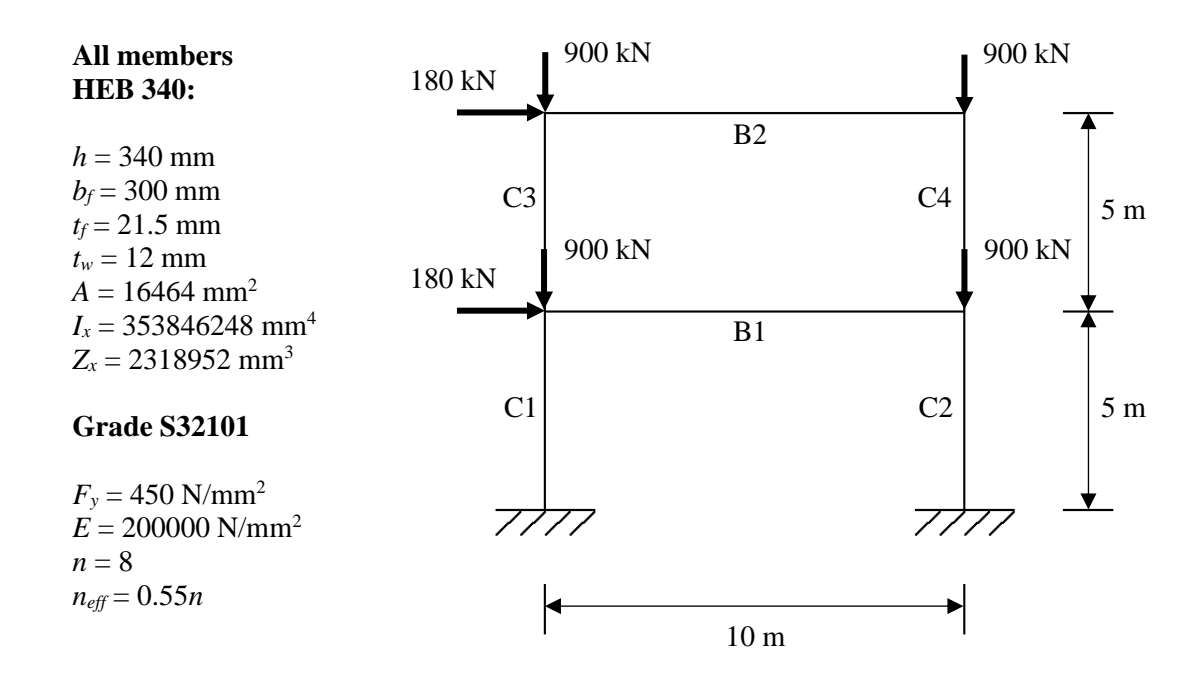


Fig. 15. Worked Example 2: Two-story duplex stainless steel frame.

**Table 1.** Ramberg-Osgood material model parameters (AISC 2020; ASCE 2020)

Material grade	Young's modulus <i>E</i> (N/mm <sup>2</sup> )	Yield (0.2% proof) stress $F_y$ (N/mm <sup>2</sup> )	Ultimate stress $F_u$ (N/mm <sup>2</sup> )	Ultimate strain $\varepsilon_u$	Strain hardening exponent <i>n</i>	Strain hardening exponent <i>m</i>
Austenitic 304	193000	205	515	0.60	7	2.1
Duplex S32101	200000	450	650	0.31	8	2.9
Ferritic 410S	200000	205	415	0.30	15	2.4

**Table 2.** Proposed  $\tau$  function coefficients

Code	Member type	$n_{eff} (\geq 2.5)$	$ au_g$	$ au_b$
	Rolled or welded I-shaped sections buckling about the minor axis, and other sections not specified in this table	0.45 <i>n</i>		
AISC 370	Rolled or welded I- shaped sections buckling about the major axis, welded box sections, and round HSS	0.55n	0.7	$\tau_b = \frac{1}{1 + 0.002 n_{eff} \frac{E}{F_y} \left(\frac{P_r}{P_{ns}}\right)^{n_{eff}-1}}$
	Rectangular HSS	n		_
ASCE-8	All sections	0.45n	0.9	_

**Table 3.** Design Cases 1 to 5 considered in this study

	Label	Analysis type	Stiffness reduction factors	Notional load coefficient	Capacity check
Design Case 1	DC1	Elastic	$ au_g +  au_b$	$0.002 (H_{NL} \text{ only})$	Member check
Design Case 2	DC2	Elastic	$ au_g$	0.002 + 0.002 $(H_{NL} + H_{ANL})$	Member check
Design Case 3	DC3	Elastic	$ au_g +  au_b$	$0.002 (H_{NL} \text{ only})$	Cross-section check
Design Case 4	DC4	Elastic	$ au_g +  au_b$	$0.002~(H_{NL}~{ m only})$	Cross-section check with CSM end points
Design Case 5	DC5	Inelastic	-	0.002 ( <i>H<sub>NL</sub></i> only)	CSM strain limit

**Table 4.** AISC 360 flexural buckling coefficients for austenitic, duplex and ferritic stainless steel (Meza, Baddoo & Gardner, 2021)

Member type	α	$eta_0$	$eta_1$	$eta_2$
Rolled or welded I-shaped sections buckling about the minor axis, and other sections not specified in this table	0.56	0.759	0.409	0.69
Rolled or welded I-shaped sections buckling about the major axis, welded box sections, and round HSS	0.58	0.891	0.455	0.82
Rectangular HSS	0.69	1.195	0.501	0.82

**Table 5.** Imperfection factors  $\alpha_{eq}$  for different types of members for calculating the equivalent member imperfection

Manhantona	Ania of husbling	$lpha_{eq}$			
Member type	Axis of buckling	Austenitic and Duplex	Ferritic		
Rectangular HSS	Any	0.49	0.34		
Round HSS	Any	0.49	0.34		
Rolled or welded I-shaped	Major	0.49	0.49		
sections, and welded box sections	Minor	0.76	0.76		

**Table 6.** Summary of comparison between the proposed AISC 370 design approaches and benchmark shell FE results for austenitic (A), duplex (D) and ferritic (F) stainless steel columns, beams and beam-columns considering Design Cases (DC) 1, 2, 3 and 5 – DC1: GNA +  $\tau_g$  +  $\tau_b$  + no member imperfections + member check, DC3: GNIA +  $\tau_g$  +  $\tau_b$  + member imperfections (L/1000) + cross-section check, DC4: GNIA +  $\tau_g$  +  $\tau_b$  + member imperfections (L/1000) + cross-section check with CSM end points, and DC5: GMNIA + member imperfections (equivalent imperfection) + CSM strain limits.

					Design by elastic analysis with stiffness reduction							Design by inelastic analysis			
	Cross-			Design Case 1		Design Case 3		Des	sign Cas	se 4	Design Case 5				
Grade	section type	Load type	No.		Radial error $R_{FE}/R_{DCI}$		Radial error RFE/RDC3			Radial error RFE/RDC4			Radial error RFE/RDC5		
				Ave.	Std.	ф	Ave.	Std.	ф	Ave.	Std.	ф	Ave.	Std.	ф
		1	55	1.01	0.06	1.08	1.00	0.09	1.04	0.97	0.09	1.00	1.03	0.05	1.09
	W-	2	55	1.08	0.07	1.15	1.06	0.09	1.12	1.03	0.09	1.08	1.03	0.05	1.10
	major	3	55	1.12	0.07	1.19	1.10	0.07	1.17	1.06	0.08	1.12	1.04	0.06	1.10
		All	165	1.07	0.08	1.13	1.05	0.09	1.10	1.02	0.10	1.06	1.03	0.05	1.10
		1	55	1.09	0.12	1.10	1.06	0.15	1.03	1.05	0.14	1.03	1.06	0.03	1.13
	W-	2	55	1.18	0.17	1.14	1.15	0.19	1.08	1.14	0.18	1.07	1.07	0.03	1.14
A	minor	3	55	1.24	0.19	1.18	1.20	0.20	1.12	1.19	0.19	1.12	1.07	0.03	1.14
		All	165	1.17	0.18	1.12	1.14	0.19	1.06	1.12	0.18	1.06	1.07	0.03	1.14
		1	55	1.02	0.09	1.07	1.00	0.11	1.03	0.97	0.10	1.00	1.06	0.06	1.13
		2	55	1.10	0.11	1.13	1.08	0.13	1.08	1.04	0.11	1.06	1.07	0.06	1.14
	SHS	3	55	1.15	0.12	1.17	1.12	0.12	1.13	1.08	0.11	1.11	1.08	0.07	1.15
		All	165	1.09	0.12	1.11	1.07	0.13	1.07	1.03	0.12	1.04	1.07	0.07	1.14
		1	33	1.02	0.06	0.96	0.98	0.06	0.93	0.99	0.06	0.93	1.01	0.03	0.95
	W-	2	33	1.09	0.06	1.02	1.04	0.06	0.98	1.05	0.06	0.99	1.02	0.04	0.96
	major	3	33	1.12	0.07	1.05	1.06	0.06	1.00	1.07	0.06	1.01	1.02	0.04	0.96
		All	99	1.08	0.07	1.01	1.03	0.07	0.97	1.04	0.07	0.98	1.02	0.04	0.96
		1	33	1.13	0.07	1.06	1.07	0.10	0.98	1.06	0.10	0.97	1.04	0.03	0.98
	W-	2	33	1.22	0.10	1.13	1.15	0.12	1.03	1.14	0.12	1.03	1.04	0.03	0.98
D	minor	3	33	1.27	0.13	1.16	1.19	0.13	1.07	1.18	0.12	1.07	1.04	0.04	0.98
		All	99	1.21	0.12	1.10	1.13	0.13	1.01	1.13	0.12	1.01	1.04	0.03	0.98
		1	33	1.04	0.04	0.98	1.02	0.05	0.96	1.00	0.05	0.94	1.05	0.04	0.99
		2	33	1.11	0.06	1.05	1.08	0.06	1.01	1.05	0.06	0.99	1.06	0.05	1.00
	SHS	3	33	1.15	0.07	1.08	1.11	0.06	1.04	1.08	0.05	1.02	1.07	0.05	1.00
		All	99	1.08	0.06	1.01	1.05	0.07	0.99	1.02	0.06	0.96	1.06	0.05	1.00
		1	55	1.03	0.06	1.09	0.99	0.07	1.04	0.94	0.08	0.99	1.03	0.05	1.10
F	F W-	2	55	1.10	0.07	1.17	1.05	0.08	1.11	1.00	0.08	1.06	1.04	0.06	1.11
	major	3	55	1.14	0.07	1.21	1.08	0.08	1.15	1.03	0.07	1.09	1.04	0.06	1.11

	All	165	1.09	0.08	1.15	1.04	0.09	1.09	0.99	0.09	1.04	1.04	0.06	1.11
	1	55	1.11	0.10	1.15	1.05	0.15	1.01	1.02	0.14	1.00	1.09	0.05	1.16
W-	2	55	1.20	0.15	1.20	1.13	0.20	1.04	1.10	0.18	1.03	1.09	0.05	1.16
minor	3	55	1.26	0.17	1.24	1.18	0.21	1.08	1.15	0.19	1.07	1.10	0.06	1.17
	All	165	1.19	0.16	1.18	1.12	0.19	1.03	1.09	0.18	1.02	1.09	0.05	1.16
	1	55	1.05	0.09	1.10	1.03	0.10	1.06	0.98	0.10	1.01	1.07	0.07	1.13
SHS	2	55	1.13	0.11	1.17	1.10	0.12	1.11	1.05	0.11	1.07	1.08	0.07	1.15
	3	55	1.18	0.11	1.22	1.14	0.12	1.16	1.09	0.11	1.12	1.09	0.07	1.15
	All	165	1.12	0.12	1.15	1.09	0.12	1.10	1.04	0.12	1.05	1.08	0.07	1.15

**Table 7.** Reliability factors considered in this study (Afshan et al. 2015, Baddoo, Meza & Gardner 2020)

	Austenitic stainless steel	Duplex stainless steel	Ferritic stainless steel
$M_m$	1.25	1.10	1.25
$V_m$	0.05	0.04	0.05
$F_m$	0.05	0.05	0.05
$V_f$	0.19	0.19	0.19

**Table 8.** Ultimate load factors  $\alpha_{DC}$  for the Vogel (1985) frame determined using Design Cases (DC) 1-5 compared against the benchmark GMNIA ultimate load factor  $\alpha_{GMNIA}$ . DC1: GNA +  $\tau_g$  +  $\tau_b$  + no member imperfections + member check, DC2: GNA +  $\tau_g$  +  $H_{ANL}$  + no member imperfections + member check, DC3: GNIA +  $\tau_g$  +  $\tau_b$  + member imperfections (L/1000) + cross-section check, DC4: GNIA +  $\tau_g$  +  $\tau_b$  + member imperfections (L/1000) + cross-section check with CSM end points, and DC5: GMNIA + member imperfections (equivalent imperfection) + CSM strain limits.

	GMNIA	DC1	DC2	DC3	DC4	DC5
$\alpha_{DC}$	1.00	0.85	0.76	0.86	0.91	1.00
$\alpha_{DC}/lpha_{GMNIA}$	-	0.85	0.76	0.86	0.91	1.00

**Table 9.** Stiffness reduction factors  $\tau_b$  calculated for members of the austenitic stainless steel Vogel (1985) frame for Design Cases 1 to 4. DC1: GNA +  $\tau_g$  +  $\tau_b$  + no member imperfections + member check, DC2: GNA +  $\tau_g$  +  $H_{ANL}$  + no member imperfections + member check, DC3: GNIA +  $t_g$  +  $t_b$  + member imperfections (L/1000) + cross-section check, and DC4: GNIA +  $t_g$  +  $t_b$  + member imperfections (L/1000) + cross-section check with CSM end points. HNL  $H_{ANL}$ 

Member	DC1	DC2	DC3	DC4
C11	0.66	-	0.66	0.63
C21	0.30	-	0.30	0.27
C31	0.53	-	0.52	0.49
B11	-	-	-	-
B21	-	-	-	-
C12	0.74	-	0.73	0.71
C22	0.40	-	0.39	0.36
C32	0.64	-	0.63	0.60
B12	-	-	-	-
B22	-	-	-	-
C13	0.82	-	0.81	0.79
C23	0.47	-	0.46	0.43
C33	0.76	-	0.75	0.73
B13	-	-	-	-
B23	-	-	-	-
C14	0.90	-	0.89	0.88
C24	0.63	-	0.63	0.60
C34	0.87	-	0.87	0.85
B14	-	-	-	-
B24	-	-	-	-
C15	0.89	-	0.88	0.87
C25	0.71	-	0.70	0.68
C35	0.87	-	0.86	0.85
B15	-	-	-	-
B25	-	-	-	-
C16	0.98	-	0.98	0.98
C26	0.95	-	0.95	0.94
C36	0.98	-	0.98	0.98
B16	-	-	-	-
B26	-	-	-	-

**Table 10.** Maximum normalised bending moments within members determined at the ultimate system loads determined for Design Cases 1 to 5 for the Vogel (1985) frame (denoted  $M_{DCI}$  to  $M_{DCS}$ ), with comparative normalised bending moments from GMNIA (denoted  $M_{GMNIA}$ ). DC1: GNA +  $\tau_g$  +  $\tau_b$  + no member imperfections + member check, DC2: GNA +  $\tau_g$  +  $H_{ANL}$  + no member imperfections + member check, DC3: GNIA +  $\tau_g$  +  $\tau_b$  + member imperfections (L/1000) + cross-section check, DC4: GNIA +  $\tau_g$  +  $\tau_b$  + member imperfections (L/1000) + cross-section check with CSM end points, and DC5: GMNIA + member imperfections (equivalent imperfection) + CSM strain limits.

Members		DC1		DC2	I	DC3		DC4		DC5
Members	$M_{DC1}/M_p$	$M_{DCI}/M_{GMNIA}$	$M_{DC2}/M_p$	$M_{DC2}/M_{GMNIA}$	$M_{DC3}/M_p$	$M_{DC3}/M_{GMNIA}$	$M_{DC4}/M_p$	$M_{DC4}/M_{GMNIA}$	$M_{DC5}/M_p$	$M_{DC5}/M_{GMNIA}$
C21	0.36	0.96	0.44	1.26	0.38	1.00	0.40	1.05	0.48	1.04
C31	0.55	1.05	0.45	0.99	0.58	1.06	0.63	1.10	0.72	1.03
B11	0.95	1.09	0.83	1.07	0.96	1.08	1.03	1.10	1.05	0.99
C22	0.38	0.96	0.35	1.04	0.40	0.97	0.43	0.98	0.54	1.01
C32	0.56	0.99	0.52	1.04	0.58	0.99	0.62	1.00	0.72	1.00
B12	0.84	1.10	0.75	1.09	0.85	1.09	0.91	1.11	0.88	0.98
C23	0.30	0.89	0.30	1.03	0.32	0.89	0.34	0.88	0.50	1.02
C33	0.54	0.97	0.48	0.99	0.55	0.96	0.59	0.96	0.70	1.00
B13	0.92	1.11	0.83	1.10	0.93	1.10	0.99	1.13	0.94	0.99
C24	0.24	0.89	0.22	0.97	0.25	0.88	0.27	0.86	0.44	1.04
C34	0.58	1.03	0.53	1.03	0.59	1.02	0.62	1.05	0.63	0.98
B14	0.85	1.21	0.76	1.16	0.86	1.20	0.92	1.24	0.79	0.99
C25	0.26	0.92	0.26	1.07	0.26	0.86	0.28	0.83	0.42	0.93
C35	0.69	0.92	0.65	0.99	0.70	0.89	0.74	0.89	0.91	0.98
B15	0.80	1.16	0.72	1.12	0.81	1.15	0.86	1.19	0.77	0.99
C26	0.09	1.23	0.08	1.27	0.09	1.17	0.09	1.16	0.09	0.92
C36	0.79	0.90	0.71	0.94	0.79	0.88	0.84	0.88	1.07	1.00
B16	0.79	1.20	0.71	1.15	0.80	1.20	0.84	1.23	0.73	1.00
Ave.		1.03		1.07		1.02		1.04		0.99
Std.		0.11		0.09		0.11		0.13		0.03
Max.		1.23		1.27		1.20		1.24		1.04
Min.		0.89		0.94		0.86		0.83		0.92

**Table 11.** Ultimate load factors of the duplex stainless steel multistory asymmetric frame determined using Design Cases 1-5  $\alpha_{DC}$  compared against the benchmark shell FE GMNIA ultimate load factor  $\alpha_{GMNIA}$ . DC1: GNA +  $\tau_g$  +  $\tau_b$  + no member imperfections + member check, DC2: GNA +  $\tau_g$  +  $H_{ANL}$  + no member imperfections + member check, DC3: GNIA +  $\tau_g$  +  $\tau_b$  + member imperfections (L/1000) + cross-section check, DC4: GNIA +  $\tau_g$  +  $\tau_b$  + member imperfections (L/1000) + cross-section check with CSM end points, and DC5: GMNIA + member imperfections (equivalent imperfection) + CSM strain limits.

	GMNIA	DC1	DC2	DC3	DC4	DC5
$\alpha_{DC}$	0.260	0.210	0.208	0.214	0.216	0.260
$lpha_{DC}/lpha_{GMNIA}$	1.00	0.81	0.80	0.82	0.83	1.00

 Table 12. Stiffness reduction factors calculated for each member in the frame for Worked Example 2.

	$ au_b$	$ au_g$
C1	0.977	0.7
C2	0.996	0.7
C3	0.997	0.7
C4	0.996	0.7
B1	-	0.7
B2	-	0.7

**Table 13.** Required compressive and flexural strengths at the critical cross-section of each member of the frame in Worked Example 2.

	$P_r$ (kN)	$M_r$ (kNm)
C1	1622.0	730.2
C2	1988.7	733.2
C3	831.9	348.3
C4	972.4	348.8
B1	92.1	560.2
B2	91.7	347.9

 Table 14. Checks on critical cross-sections of six frame members in Worked Example 2

C1	$\frac{1622.0}{6667.9} + \frac{8730.2}{939.2} = 0.93$	$0.93 \le 1 \div \text{ok}$
C2	$\frac{1988.7}{6667.9} + \frac{8733.2}{939.2} = 0.99$	$0.99 \le 1 \div \text{ok}$
C3	$\frac{831.9}{2(6667.9)} + \frac{348.3}{939.2} = 0.43$	$0.43 \le 1 \div \text{ok}$
C4	$\frac{972.4}{2(6667.9)} + \frac{348.8}{939.2} = 0.44$	$0.44 \le 1 \div \text{ok}$
B1	$\frac{92.1}{2(6667.9)} + \frac{560.2}{939.2} = 0.60$	$0.60 \le 1 \div \text{ok}$
B2	$\frac{91.7}{2(6667.9)} + \frac{347.9}{939.2} = 0.38$	0.38 ≤ 1 ∴ ok